

Convolutional Neural Networks for Classification of Alzheimer's Disease: Overview and Reproducible Evaluation

Junhao Wen^{a,b,c,d,e*}, Elina Thibeau--Sutre^{a,b,c,d,e*}, Jorge Samper-González^{e,a,b,c,d}, Alexandre Routier^{e,a,b,c,d}, Simona Bottani^{e,a,b,c,d}, Stanley Durrleman^{e,a,b,c,d}, Ninon Burgos^{a,b,c,d,e}, Olivier Colliot^{a,b,c,d,e,f,†}, for the Alzheimer's Disease Neuroimaging Initiative¹ and the Australian Imaging Biomarkers and Lifestyle flagship study of ageing²

^a*Institut du Cerveau et de la Moelle épinière, ICM, F-75013, Paris, France*

^b*Sorbonne Université, F-75013, Paris, France*

^c*Inserm, U 1127, F-75013, Paris, France*

^d*CNRS, UMR 7225, F-75013, Paris, France*

^e*Inria, Aramis project-team, F-75013, Paris, France*

^f*AP-HP, Hôpital de la Pitié Salpêtrière, Department of Neurology and Neuroradiology, F-75013, Paris, France*

*denotes shared first authorship

†Corresponding author:

Olivier Colliot, PhD - olivier.colliot@upmc.fr

ICM – Brain and Spinal Cord Institute

ARAMIS team

Pitié-Salpêtrière Hospital

47-83, boulevard de l'Hôpital, 75651 Paris Cedex 13, France

¹ Data used in preparation of this article were obtained from the Alzheimer's Disease Neuroimaging Initiative (ADNI) database (adni.loni.usc.edu). As such, the investigators within the ADNI contributed to the design and implementation of ADNI and/or provided data but did not participate in analysis or writing of this report. A complete listing of ADNI investigators can be found at: http://adni.loni.usc.edu/wp-content/uploads/how_to_apply/ADNI_Acknowledgement_List.pdf

² Data used in the preparation of this article was obtained from the Australian Imaging Biomarkers and Lifestyle flagship study of ageing (AIBL) funded by the Commonwealth Scientific and Industrial Research Organisation (CSIRO) which was made available at the ADNI database (www.loni.usc.edu/ADNI). The AIBL researchers contributed data but did not participate in analysis or writing of this report. AIBL researchers are listed at www.aibl.csiro.au.

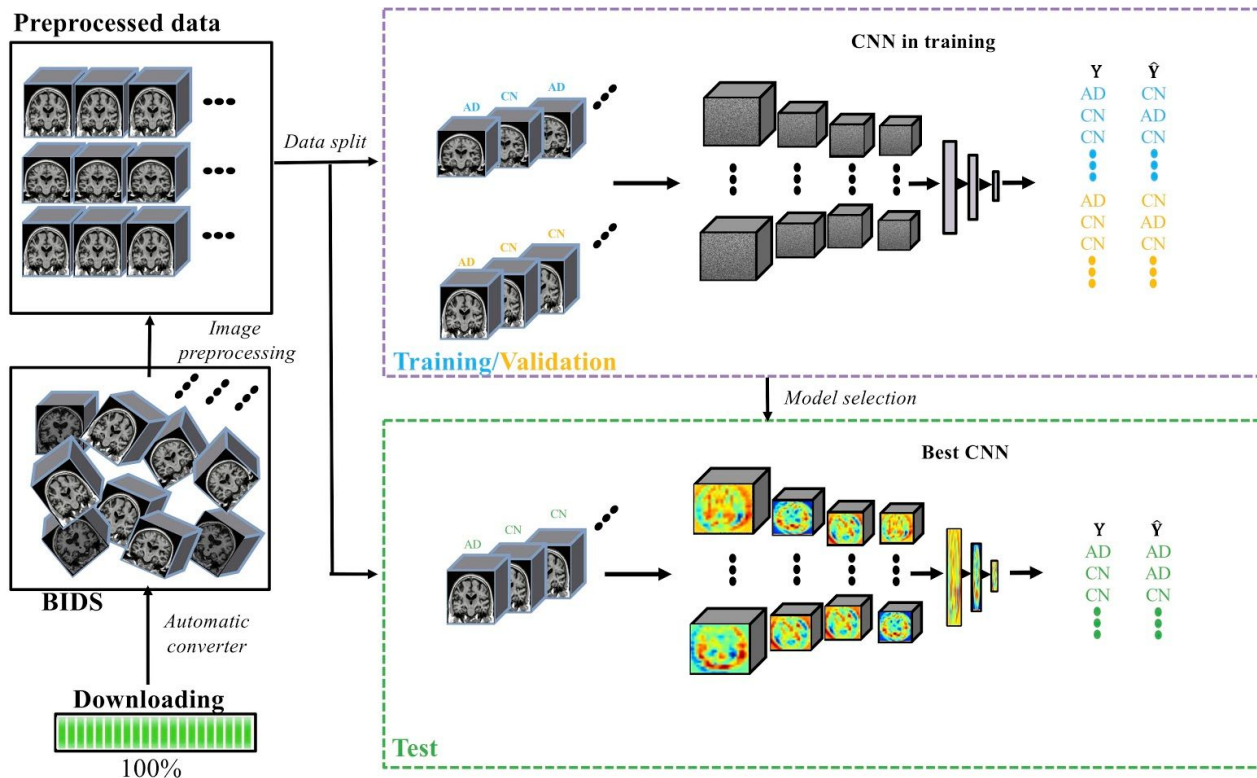
Note to the editor and reviewers:

The evaluation of the models involves a separation into training/validation and test sets. The test set was separated from the very beginning and concealed. It was left untouched (we have not yet evaluated the models on the test set) and will be until the end of the review process. This was done to avoid overfitting the test set when trying different architectures or hyperparameters, either during the currently presented experiments or during the possible additional experiments that could be asked by the reviewers. Once the review process has converged to an agreement among reviewers and editor about the possible changes to architecture and hyperparameters, we will evaluate the best model for each category on the test data and quantify the models' performance and generalization ability. By doing this, we hope to improve the transparency of our research. As a result, parts which are marked in red will be modified after the peer-review.

Highlights

- We systematically and critically reviewed the state-of-the-art, hoping to draw the attention of the community on existing bad practices;
- We proposed an open-source framework for reproducible evaluation of classification in Alzheimer's disease based on convolutional neural networks and T1-weighted MRI;
- We demonstrated the use of the proposed framework on three public datasets: training/validating and testing both on ADNI or training/validating on ADNI and testing on independent datasets (AIBL and OASIS);
- We studied the influence of key components on classification performances and benchmarked a baseline performance for future studies.

Graphical abstract



Abstract

Early and accurate diagnosis of Alzheimer's disease (AD) is an important and challenging task. Numerous studies have proposed to address this challenge using machine learning (ML) from brain imaging data. In particular, in the past two years, over 30 papers have proposed to use convolutional neural network (CNN) for AD classification. However, the classification performances across studies are difficult to compare due to variations in components such as participant selection, image preprocessing or validation procedure. Moreover, these studies are hardly reproducible because their frameworks are not publicly accessible and because implementation details are lacking. Lastly, some of these papers may reported biased performances due to inadequate or unclear validation procedure and also it is unclear how the model architecture and parameters were chosen. In the present work, we aim to address these limitations through three main contributions. First, we performed a systematic literature review of studies using CNN for AD classification from anatomical MRI. We identified four main types of approaches: i) 2D slice-level, ii) 3D patch-level, iii) ROI-based and iv) 3D subject-level CNN. Moreover, we found that more than half of the surveyed papers may have suffered from data leakage and thus reported biased performances. Our second contribution is an open-source framework for classification of AD using CNN and T1-weighted MRI. The framework comprises: tools to automatically convert ADNI, AIBL and OASIS data into the BIDS standard, a modular set of image preprocessing procedures, classification architectures and an evaluation framework. Thirdly, we used this framework to rigorously compare different CNN architectures, which are representative of the existing literature, and to study the influence of key components on classification performances. Importantly, the data was split into training/validation/test sets at the very beginning. Training/validation sets were used in a CV procedure for model selection. To avoid any overfitting of the test sets by testing different architectures, hyperparameters or preprocessing, the test sets were left untouched until the end of the peer-review procedure. We included three test sets: one from ADNI to assess generalization to different patients from the same study, one from AIBL for generalization to a different study but with similar imaging protocols and inclusion criteria, one from OASIS to assess generalization to different protocols and inclusion criteria. [Results will be modified after peer-review]. On the validation set, the ROI-based (hippocampus) CNN achieved highest balanced accuracy (0.86 for AD vs CN and 0.80 for sMCI vs pMCI) compared to other approaches. Transfer learning with autoencoder pre-training did not improve the average accuracy but reduced the variance. Training using longitudinal data resulted in similar or higher performance, depending on the approach, compared to training with only baseline data. Sophisticated image preprocessing did not improve the results. Lastly, CNN performed similarly to standard SVM for task AD vs CN but outperformed SVM for task sMCI vs pMCI, demonstrating the potential of deep learning for challenging diagnostic tasks. All the code of the framework and the experiments is publicly available: general-purpose tools have been integrated into the Clinica software (www.clinica.run) and the paper-specific code is available at: <https://gitlab.icm-institute.org/aramislab/AD-ML>.

Keywords: convolutional neural network, reproducibility, Alzheimer's disease classification, magnetic resonance imaging

1. Introduction

Alzheimer's disease (AD), a chronic neurodegenerative disease causing the death of nerve cells and tissue loss throughout the brain, usually starts slowly and worsens over time (McKhann et al., 1984). AD is expected to affect 1 out of 85 people in the world by the year 2050 (Brookmeyer et al., 2007). The cost of caring for AD patients is also expected to raise dramatically, thus the need of individual computer-aided systems for early and accurate AD diagnosis.

Magnetic resonance imaging (MRI) offers the possibility to study pathological brain changes associated with AD *in vivo* (Ewers et al., 2011). Over the past decades, neuroimaging data have been increasingly used to characterize AD by means of machine learning (ML) methods, offering promising tools for individualized diagnosis and prognosis (Falahati et al., 2014; Haller et al., 2011; Rathore et al., 2017). A large number of studies have proposed to use predefined features (including regional and voxel-based measurements) from image preprocessing pipelines followed by different types of classifiers, such as support vector machines (SVM) or random forests. Such approach is often referred to as conventional ML (LeCun et al., 2015). More recently, deep learning (DL), as a newly emerging ML methodology, has made a big leap in the domain of medical imaging (Bernal et al., 2018; J. Liu et al., 2018; Lundervold and Lundervold, 2018; Razzak et al., 2018; D. Wen et al., 2018). As the most widely used architecture of DL, convolutional neural network (CNN) has attracted huge attention due to its great success in image classification (Krizhevsky et al., 2012). Contrary to conventional ML, DL allows the automatic abstraction of low-to-high level latent feature representations (e.g. lines, dots, or edges for low level features, and objects or larger shapes for high level features). Thus, one can hypothesize that DL depends less on image preprocessing and requires less prior on other complex procedures, such as feature selection, resulting in a more objective and less bias-prone process (LeCun et al., 2015).

Very recently, numerous studies have proposed to assist diagnosis of AD by means of CNNs (Aderghal et al., 2018, 2017a, 2017b; Bäckström et al., 2018; Basaia et al., 2019; Cheng et al., 2017; Cheng and Liu, 2017; Farooq et al., 2017; Gunawardena et al., 2017; Hon and Khan, 2017; Hosseini Asl et al., 2018; Islam and Zhang, 2018, 2017; Korolev et al., 2017; Lian et al., 2018; Li et al., 2018, 2017; Lin et al., 2018; Manhua Liu et al., 2018; Mingxia Liu et al., 2018a, 2018c; Qiu et al., 2018; Senanayake et al., 2018; Shmulev et al., 2018; Taqi et al., 2018; Valliani and Soni, 2017; Vu et al., 2018, 2017; Wang et al., 2019, 2017; S.-H. Wang et al., 2018; Wu et al., 2018). However, classification performances among these studies are not directly comparable because they differ in terms of: i) sets of participants; ii) image preprocessing procedures, iii) cross-validation (CV) procedure and iv) reported evaluation metrics. It is thus impossible to determine which approach performs best. The generalization ability of these approaches also remains unclear. In DL, the use of fully independent test sets is even more critical than in conventional ML, because of the very high flexibility with numerous possible model architecture and training hyperparameter choices. Assessing generalization to other studies is also critical to ensure that the characteristics of the considered study have not been overfitted. In previous works, the generalization may be questionable due to: i) inadequate validation procedures, ii) absence of independent test set, or iii) test set chosen from the same study.

In our previous studies (Samper-González et al., 2018; J. Wen et al., 2018), we have proposed an open source framework for reproducible evaluation of AD classification using conventional ML methods. The framework comprises: i) tools to automatically convert three publicly available datasets into the Brain Imaging Data Structure (BIDS) format (Gorgolewski et al., 2016) and ii) a modular set of preprocessing pipelines, feature extraction and classification methods, together with an evaluation framework, that provide a baseline for benchmarking the different components. We demonstrated the use of this framework on positron emission tomography (PET), T1-weighted (T1w) MRI (Samper-González et al., 2018) and diffusion MRI data (J. Wen et al., 2018).

In the present work, we extended the framework to DL approaches using CNNs. We first reviewed and summarized the different studies using CNNs and anatomical MRI for AD classification. In particular, we reviewed their validation procedures and the possible presence of data leakage. Then, different CNN architectures were implemented in our open source framework. We compared the performance of these

approaches and studied the influence of key components on the classification performance. The proposed CNNs were also compared to a conventional ML approach based on a linear SVM. Lastly, we assessed the generalization ability of the CNN models within (training and testing on ADNI) and across datasets (training on ADNI and testing on AIBL or OASIS).

All the code of the framework and the experiments is publicly available: general-purpose tools have been integrated into Clinica³ (Routier et al., 2018), an open-source software platform that we developed to process data from neuroimaging studies, and the paper-specific code is available at: <https://gitlab.icm-institute.org/aramislab/AD-ML>.

³ <http://www.clinica.run/>

2. Background

Designing DL approaches for MRI-based classification of AD requires expertise about DL, MRI processing and AD. Such knowledge might be difficult to acquire for newcomers to the field and, as we will see from the state-of-the-art, its lack may lead to flaws in the proposed approaches. This section introduces the basic concepts regarding: i) the key aspects of DL, including the main building layers of CNN, classical CNN architectures and methods to tackle the overfitting problem; ii) the main preprocessing steps for anatomical MRI; iii) fundamental goals and tasks in application of AD. Readers should feel free to skip this section given their background and knowledge. Conversely, for more details, see (Goodfellow et al., 2016) about DL and (Bankman, 2008) for MRI processing.

2.1. Convolutional neural networks

2.1.1. Main building layers of CNN

CNNs are the most widely used type of network for computer vision and image analysis. A CNN is made of an input and an output layer, as well as different hidden layers. The hidden layers typically include convolutional layers, pooling layers, activation functions and fully connected (FC) layers.

The convolutional layer is the core building block of a CNN. It acts as an automatic feature extractor (on the contrary, conventional ML methods would typically use hand-craft feature extraction or selection). Convolutional layers apply learnable filters to all available receptive fields with a convolutional operation. A filter or kernel is a 2D (or 3D for MRI) matrix of weights. A receptive field is a local patch of the input image, of the same size as the filter. The filter is convolved with all the local receptive fields. The application of a given filter to the whole input image generates a feature map or activation map. All the feature maps are then stacked to constitute the output volume of a convolutional layer. Several hyperparameters (number of filters, stride size and padding size) control the size of the output volume (see (Dumoulin and Visin, 2016) for more details).

Another building block of CNNs is the pooling layer, which reduces the dimensionality of the feature maps. The pooling layer combines the outputs of a cluster of neurons of the current layer into a single neuron in the next layer (Ciresan et al., 2011; Krizhevsky et al., 2012). Pooling can be of different types, such as max, average and sum pooling (Scherer et al., 2010).

To learn a mapping between the adjacent convolutional layers, one applies activation functions to the output volume of each convolutional layer. The rectified linear unit (ReLU) is the most common activation function and ensures a sparse and non-linear representation (Glorot et al., 2011; Krizhevsky et al., 2012; Nair and Hinton, 2010). However, ReLU can be fragile during backpropagation. Indeed, the fact that ReLU sets all negative values to be zero can cause the problem of gradient vanishing or dying ReLU. If this happens, the gradient flowing through the unit will be forever zero during backpropagation. One alternative, leaky ReLU, can overcome this drawback by introducing a small negative slope (e.g. 0.01), thus allowing a small positive gradient when the unit is not active (Maas et al., 2013).

FC layers learn the relationship between the features, extracted by previous convolutional and pooling layers, and the target (in our case the patient's diagnosis). In a FC layer, all the neurons in the current layer are connected to all the neurons in the previous layer. The output volumes (one for each feature map) from the previous convolutional layers are first flattened and then fed as input to the FC. For a n-class classification problem, the output of the last FC layer is composed of n neurons which values indicate membership to a given class. This can be transformed into n probabilities by using a softmax function on the outputs (Goodfellow et al., 2016).

The loss function is used to measure the difference between the predicted and true labels. Cross entropy loss, measuring the distance between the output distribution and the real distribution, is widely used in

classification tasks (de Boer et al., 2005). Other loss functions were also discussed in the literature, such as mean squared error (MSE) loss and hinge loss (see (Janocha and Czarnecki, 2017) for details).

The weights and biases of the network are learned using an optimization algorithm, such as the stochastic gradient descent (SGD). Most often, backpropagation is used to successively update the weights of the different layers.

2.1.2. Classical CNN architectures

Several CNN architectures have become classical, often due to their performance on the ImageNet Large Scale Visual Recognition Challenge (ILSVRC): a benchmark in object category classification and detection on hundreds of object categories and millions of images (Deng et al., 2009). These architectures were originally designed for 2D natural images. However, some of them have been adapted to the applications of MRIs.

Before the ILSVRC that began in 2010, Yann Lecun proposed LeNet-5 to recognize handwritten digits from the MNIST database (Lecun et al., 1998). This network includes seven layers: two convolutional layers associated with pooling layers, followed by three FC layers.

In 2012, AlexNet (Krizhevsky et al., 2012) significantly outperformed all the prior competitors of the ILSVRC, reducing the top-5 error from 26% to 15.3%. The network went deeper than LeNet-5, with more filters per layer. It consisted of five convolutional layers with decreasing filter size (11x11, 5x5 and 3x3) and three FC layers.

The runner-up at ILSVRC 2014 was VGGNet (Simonyan and Zisserman, 2014), which consists of 16 convolutional layers. It was appealing because of its uniform architecture, including only 3x3 convolutional filters cross the entire architecture. One of the main conclusion of this architecture is that using many small filters of size 3x3 is more efficient than using only a few filters of bigger size. The winner of that year was GoogleNet or Inception V1 (Szegedy et al., 2015). It went deeper (22 layers) and achieved a top-5 error rate of 6.67%. This architecture was inspired by LeNet-5 and implemented a novel element called the inception layer. The idea behind the inception layer is to convolve over larger receptive fields, but also keep a fine resolution based on smaller receptive fields. Thus, different filter sizes (from 1x1 to 5x5) were used in the same convolutional layer.

ILSVRC 2015 was won by the Residual Neural Network (ResNet) (He et al., 2016) with a top-5 error rate of 3,57%. ResNet includes over a hundred layers by introducing a novel architecture with shortcut connections that perform identity mapping and heavy batch normalization. Such shortcut connections make the deep residual nets easier to optimize than their counterpart “plain” nets.

DenseNet was presented at ILSVRC 2016 (Huang et al., 2017). It introduces the so-called dense block: each layer receives the outputs of all previous layers as input. The underlying assumption of dense connectivity is that each layer should have access to all the preceding feature maps and this “collective knowledge” therefore helps to improve the performance. In the same way than ResNet, dense connectivity allows the construction of very deep CNNs, such as DenseNet-264 which consists of 264 layers.

2.1.3. Methods to deal with overfitting

Neuroimaging datasets of AD patients are usually of relatively small size (typically a few hundreds of samples) compared, for instance, to those in computer vision (typically several million). DL models tend to easily overfit when trained on small samples due to the large number of learnt parameters (Goodfellow et al., 2016). Here, we summarize the main strategies to alleviate overfitting.

Data augmentation aims at generating new data samples from the available training data (Perez and Wang, 2017). It can be categorized into: i) transformation methods, which apply a combination of simple transformations (e.g. rotation, distortion, blurring and flipping) on the training data and ii) data synthesis methods, which aim to learn the training distribution to then generate new samples. Data synthesis often relies

on autoencoders (AE) (Bouillard and Kamp, 1988; Hinton and Zemel, 1994; Yann, 1987) and Generative Adversarial Networks (GANs) (Goodfellow, 2016).

Dropout randomly and independently drops neurons, setting their output value to be zero along with their connections (Srivastava et al., 2014). This aims to make the network less complex and thus less prone to overfitting.

Another approach involves a regularization of the weights which makes the model less complex. This enhances the generalizability of the model. In DL, a common regularization is weight decay, where the updated weights are regularized by multiplying by a factor slightly smaller than 1 (Krogh and Hertz, 1992).

Batch normalization is a procedure which normalizes the input of a given set of layers (the normalization is done using the mean and standard-deviation of a batch, hence the name) (Ioffe and Szegedy, 2015). This procedure acts as a regularizer, in some cases eliminating the need for dropout (Ioffe and Szegedy, 2015). In addition, it helps battle against the gradient explosion phenomenon and allows using much higher learning rates and being less careful about initialization (Panigrahi et al., 2018).

Transfer learning is a broadly defined terminology. In general, it consists in using a model trained on a given task, called the source task (e.g. ImageNet classification task or unsupervised learning task), in order to perform a target task (e.g. AD classification). Here, we introduce two transfer learning approaches that have been used in the context of AD classification. The first one is based on performing unsupervised learning before the supervised learning on the task of interest. It is supposed to be useful when one has limited labeled data but a larger set of unlabeled data. In that case, the most common approach is to use an AE (Yann, 1987). Strictly speaking, the AE is made of two parts: an encoder layer and a decoder layer. Generally, several AEs are stacked, the resulting being called stacked AE, but which we will refer to as AE for the sake of simplicity. The encoder learns to compress the original data and produces a representation, the decoder then reconstructs the input using only this representation. An illustration of AE is shown in Figure 1. The weights and biases of the target network (e.g. CNNs) are then initialized with those of the encoder part of AE, which should provide a better initialization. The second approach involves transferring a model trained on ImageNet to the problem of classification of AD. As for the AE, the weights and biases of the target network are initialized with those of the source network. The idea behind is that random weight initialization of DL models may place parameters in a region of the parameter space where poor generalization occurs, while transfer learning may provide a better initialization (Erhan et al., 2010).

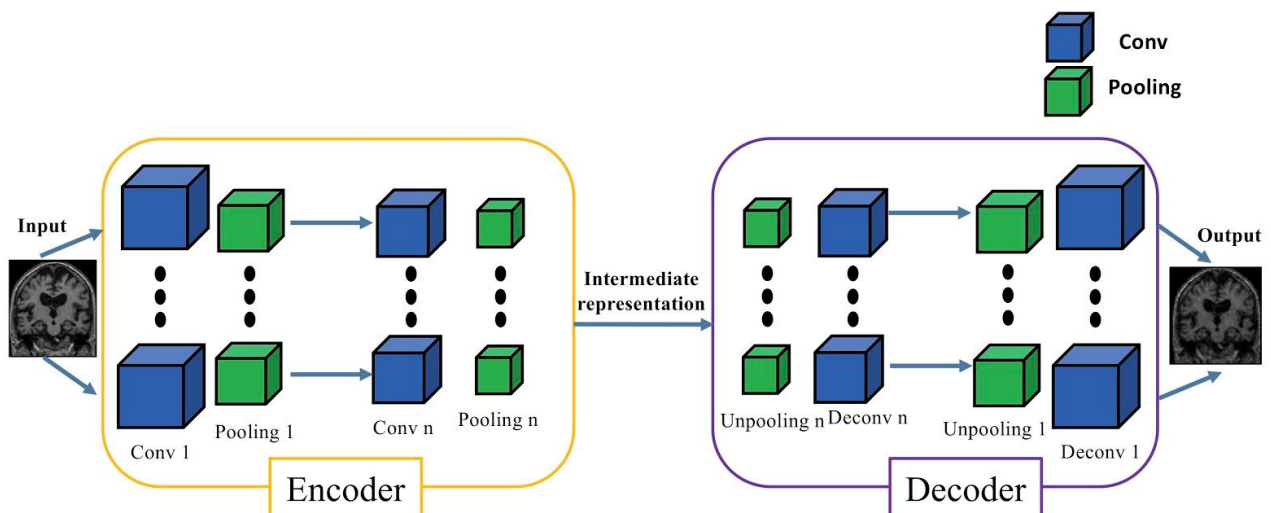


Figure 1. The architecture of a stacked AE made up of n AEs. For the n -th AE, the encoder part is made of one convolutional layer (Conv n), one pooling layer (Pooling n) and one activation function, sequentially. Correspondingly, the decoder part consists of one activation function, one unpooling layer (Unpooling n) and one deconvolutional layer (Deconv n), sequentially. The n AEs's encoder and decoder parts are separated and then stacked to construct the final stacked AE. This layer-wise fashion ensures that the output of the former

AE's encoder/decoder connects as input for the next AE's encoder/decoder. The intermediate representation provides a reduced representation of the data.

Early Stopping consists in stopping the learning process at an earlier point. It aims to determine the number of epochs (or iterations) at which the network should be stopped before being severely overfitted. For instance, one can select the model parameters corresponding to the lowest validation error rather than the last updated parameters. Various other stopping criteria have been proposed (Prechelt, 2012; Yao et al., 2007; Zhang and Yu, 2005).

2.2. MRI preprocessing

A proper image preprocessing procedure is a fundamental step to ensure a good classification performance, especially in the domain of MRI (Cuingnet et al., 2011; Lu and Weng, 2007; Uchida, 2013). Although CNNs have the potential to extract low-to-high level features from the raw images, the influence of image preprocessing remains to be clarified. We present here the essential steps for MR image processing in the context of AD classification.

2.2.1. Bias field correction

MR images can be corrupted by a low frequency and smooth signal caused by magnetic field inhomogeneities. This bias field induces variations in the intensity of the same tissue in different locations of the image, which deteriorates the performance of image analysis algorithms such as registration (Vovk et al., 2007). Several methods exist to correct these intensity inhomogeneities, two popular ones being the nonparametric nonuniformity intensity normalization (N3) algorithm (Sled et al., 1998), available for example in the Freesurfer software package⁴, and the N4 algorithm (Tustison et al., 2010) implemented in ITK⁵.

2.2.2. Intensity rescaling and standardization

As MRI is usually not a quantitative imaging modality, MR images usually have different intensity ranges and the intensity distribution of the same tissue type may be different between two images, which might affect the subsequent image preprocessing steps. The first point can be dealt with by globally rescaling the image, for example between 0 and 1 using the minimum and maximum intensity values (Juszczak et al., 2002). Intensity standardization can be achieved using techniques such as histogram matching (Madabhushi and Udupa, 2005).

2.2.3. Skull stripping

Extracranial tissues can be an obstacle for image analysis algorithms (Kalavathi and Prasath, 2016). A large number of methods have been developed for brain extraction, also called skull stripping, and many are implemented in software tools, such as the Brain Extraction Tool (BET) (Smith, 2002) available in FSL⁶, or the Brain Surface Extractor (BSE) (Shattuck et al., 2001) available in BrainSuite⁷. These methods are often sensitive to the presence of noise and artifacts, which can result in over or under segmentation of the brain.

2.2.4. Image registration

Medical image registration consists of spatially aligning two or more images, either globally (rigid and affine registration) or locally (non-rigid registration), so that voxels in corresponding positions contain comparable information. A large number of software tools have been developed for MRI-based registration (Oliveira and Tavares, 2014). FLIRT⁸ (Greve and Fischl, 2009; Jenkinson et al., 2002; Jenkinson and Smith, 2001) and

⁴ <http://surfer.nmr.mgh.harvard.edu/fswiki/recon-all>

⁵ <http://hdl.handle.net/10380/3053>

⁶ <https://fsl.fmrib.ox.ac.uk/fsl/fslwiki/BET/UserGuide>

⁷ <http://brainsuite.org/processing/surfaceextraction/bse>

⁸ <https://fsl.fmrib.ox.ac.uk/fsl/fslwiki/FLIRT>

FNIRT⁹ (Andersson et al., 2010) are FSL tools dedicated to linear and non-linear registration, respectively. The Statistical Parametric Mapping (SPM) software package¹⁰ and Advanced Normalization Tools¹¹ (ANTs) also offer solutions for both linear and non-linear registration (Ashburner and Friston, 2000; Avants et al., 2014; Friston et al., 1995).

2.3. Classification of AD

2.3.1. Main classification tasks

Early and accurate diagnosis of AD is difficult, partly because of the large number of measures involved, such as neuroimaging and fluid biomarkers or neuropsychological tests. The ability of DL algorithms to learn relevant patterns within the data is expected to enable accurate automatic classifications and predictions.

A first objective can be to differentiate patients with AD from cognitively normal subjects (CN). Even though its clinical relevance is limited, the AD vs CN task is widely used to assess the performances of classification methods and to compare them. It can also be used as an initialization before performing a more complex task.

Before the development of dementia, patients go through a phase called mild cognitive impairment (MCI) during which they have objective deficits but not severe enough to result in dementia. A second objective can be to identify the early stage of AD by differentiating CN subjects from MCI patients (CN vs MCI).

Patients with MCI may remain stable or subsequently progress to AD dementia or to another type of dementia. Distinguishing MCI subjects that will progress to AD (denoted as pMCI) from those who will remain stable (denoted as sMCI) would allow predicting the group of subjects that will likely develop the disease. pMCI subjects could then be included into clinical trials. The sMCI vs pMCI task requires a longitudinal follow-up of the subjects. When longitudinal data are not available, a proxy task consists of distinguishing subjects at an early stage of the MCI phase (EMCI) from subjects at a late stage (LMCI). However, the EMCI and LMCI labels are not as robust as sMCI and pMCI to predict the conversion because the stability of the diagnosis is not guaranteed.

2.3.2. Main datasets used for AD classification

Three publicly available datasets have been mainly used for the study of AD: the Alzheimer's Disease Neuroimaging Initiative (ADNI), the Australian Imaging, Biomarkers and Lifestyle (AIBL) and the Open Access Series of Imaging Studies (OASIS). In the following, we briefly describe these datasets and provide explanations on the diagnosis labels provided. Indeed, the diagnostic criteria of these studies differ, hence there is no strict equivalence between the labels of ADNI and AIBL, and those of OASIS.

The ADNI study is composed of 4 cohorts: ADNI-1, ADNI-GO, ADNI-2 and ADNI-3. These cohorts are dependant and longitudinal, meaning that one cohort may include the same patient more than once and that different cohorts may include the same patients. Many modalities are included in these datasets including clinical, genetic, imaging (MRI and PET) data, as well as biospecimen analyses such as blood, urine and cerebrospinal fluid (CSF). Diagnosis labels are given by a physician after a series of tests (Petersen et al., 2010). The existing labels are:

- AD (Alzheimer's disease): mildly demented patients,
- MCI (mild cognitive impairment): patients in the prodromal phase of AD,
- NC (normal controls): elderly control participants,

⁹ <https://fsl.fmrib.ox.ac.uk/fsl/fslwiki/FNIRT>

¹⁰ <https://www.fil.ion.ucl.ac.uk/spm>

¹¹ <http://stnava.github.io/ANTs>

- SMC (significant memory concern): participants with cognitive complaints and no pathological neuropsychological findings. The designations SMC and subjective cognitive decline (SCD) are equivalently found in the literature.

Since the ADNI-GO and ADNI-2 cohorts, new patients at the very beginning of the prodromal stage have been recruited (Aisen et al., 2010), hence the MCI label has been split into two labels:

- EMCI (early MCI): patients at the beginning of the prodromal phase,
- LMCI (late MCI): patients at the end of the prodromal phase (similar to the previous label MCI of ADNI-1).

This division is made on the basis of the score obtained on memory tasks corrected by the education level. However, both classes remain very similar and they are fused in many studies under the MCI label.

The AIBL project includes a longitudinal cohort of patients. Several modalities are present in the dataset, such as clinical and imaging (MRI and PET) data, as well as the analysis of blood and CSF samples. As in ADNI, the diagnosis is given according to a series of clinical tests (Ellis et al., 2010, 2009) and the existing labels are AD, MCI and NC.

The OASIS project includes three cohorts, OASIS-1, OASIS-2 and OASIS-3. The first cohort OASIS-1 is only cross-sectional, whereas the other two are longitudinal. Available data is far more limited than in ADNI with only few clinical tests and imaging data (MRI and PET only in OASIS-3). Diagnosis labels are given only based on the clinical dementia rating (CDR) scale (Marcus et al., 2007). Two labels can be found in the OASIS-1 dataset:

- AD, which corresponds to patients with a non-null CDR score. This class gathers patients who would be spread between the MCI and AD classes in ADNI. A subdivision of this class is done based on the CDR, the scores of 0.5, 1, 2 and 3 representing very mild, mild, moderate and severe dementia, respectively.
- Control, which corresponds to patients with a CDR of zero. Unlike ADNI, some of the controls are younger than 55.

In many datasets, the label related to the stability of the diagnosis (i.e. sMCI and pMCI) is not given in the baseline data and must be deduced from the longitudinal data. The way these labels were defined in our study is described in the Materials section and its implementation is available at: <https://gitlab.icm-institute.org/aramislab/AD-ML>.

Note that some of the image preprocessing steps described in section 2.2 may have already been performed by the dataset provider. However, different preprocessing pipelines can be run on the same dataset, so the name of the dataset does not provide sufficient information to know which methods have been applied to the data. It is thus crucial to describe all the preprocessing steps applied to the subjects' images.

3. State of the art

We performed an online search of publications concerning classification of AD using neural networks based on anatomical MRI in PubMed and Scopus, from January 1990 to the 15th of January 2019. This resulted in 406 records which were screened according to their abstract, type and content (more details are provided in online supplementary eMethod 1) to retain only those focused on the classification of AD stages using at least anatomical MRI as input of a neural network. This resulted in 71 studies. Out of these 71, 32 studies used CNN on image data in an end-to-end framework, which is the focus of our work. We found that a substantial proportion of these studies performed a biased evaluation of results, due to the presence of data leakage, hence we first discuss the data leakage issues that we encountered in our bibliography (Section 3.1). We then review the 32 studies that used end-to-end CNNs on image data, the main focus of this work (Section 3.2). Finally, we briefly describe other studies that were kept in our bibliography but that are out of our scope (Section 3.3).

3.1. Main causes of data leakage

Unbiased evaluation of classification algorithms is critical to assess their potential clinical value. A major source of bias is data leakage, which refers to the use of test data in any part of the training process (Kriegeskorte et al., 2009; Rathore et al., 2017). Data leakage can be difficult to detect for DL approaches as they can be complex and very flexible. We assessed the prevalence of data leakage among the papers described in section 3.2 and analyzed its causes. The articles were labeled into three categories: i) *Clear* when data leakage was explicitly witnessed; ii) *Unclear* when no sufficient explanation was offered and iii) *None detected*. The results are summarized in the last of column of Table 1. They were further categorized according to the cause of data leakage. Four main causes were identified:

- 1. Wrong data split.** Not splitting the dataset at the subject-level when defining the training, validation and test sets can result in data from the same subject to appear in several sets. This problem can occur when patches or slices are extracted from a 3D image, or when images of the same subject are available at multiple time points. (Bäckström et al., 2018) showed that, using a longitudinal dataset, a biased dataset split (at the image level) can result in an accuracy increase of 8 percent points compared to an unbiased split (at the subject-level).
- 2. Late split.** Procedures such as data augmentation, feature selection or AE pre-training must never use the test set and thus be performed after the training/validation/test split to avoid biasing the results. For example, if data augmentation is performed before isolating the test data from the training/validation data, then images generated from the same original image may be found in both sets, leading to a problem similar to the wrong data split.
- 3. Biased transfer learning.** Transfer learning can result in data leakage when the source and target domains overlap, for example when a network pre-trained on the AD vs CN task is used to initialize a network for the MCI vs CN task and that the CN subjects in the training or validation sets of the source task (AD vs CN) are also in the test set of the target task (MCI vs CN).
- 4. Absence of an independent test set.** The test set should only be used to evaluate the final performance of the classifier, not to choose the training hyperparameters (e.g. learning rate) of the model. A separate validation set must be used beforehand for hyperparameter optimization.

Note that we did not consider data leakage occurring when designing the network architecture, possibly chosen thanks to successive evaluations on the test set, as the large majority of the studies does not explicit this step.

All these data leakage causes may not have the same impact on data performance. For instance, it is likely that a wrong data split in a longitudinal dataset or at the slice-level is more damaging than a late split for AE pre-training.

3.2. Classification of AD with end-to-end CNNs

This section focuses on CNNs applied to an Euclidean space (here a 2D or 3D image) in an end-to-end framework (from the input to the classification). A summary of these studies can be found in Table 1. The table indicates whether data leakage was potentially present, which can have biased the performance upwards. Below, we categorized studies according to the type of input of the network: i) 2D slice-level, ii) 3D patch-level, iii) ROI-based and iv) 3D subject-level.

Table 1. Summary of the studies performing classification of AD using CNNs on anatomical MRI. Studies are categorized according to the potential presence of data leakage: (A) studies without data leakage; (B) studies with potential data leakage.

Types of data leakage if presented: a, Wrong dataset split; b, Absence of independent test set; c, Late split; d, Biased transfer learning (see Section 3.1).

* In (Bäckström et al., 2018), data leakage was introduced on purpose in order to study its influence. Thus, this study is present in both categories.

† Use of imbalanced accuracy on a severely imbalanced dataset (one class is less than half of the other), leading to an over-optimistic estimation of performance.

1: accuracy; 2: balanced accuracy.

(A) None detected Table

Study	Performance					Approach	Data leakage
	AD vs CN	sMCI vs pMCI	MCI vs CN	AD vs MCI	Multi-class		
(Aderghal et al., 2017b)	0.84 ¹	--	0.65 ¹	0.67 ^{1†}	--	ROI-based	None detected
(Aderghal et al., 2018)	0.90 ²	--	0.73 ²	0.83 ²	--	ROI-based	None detected
(Bäckström et al., 2018) *	0.90 ¹	--	--	--	--	3D subject-level	None detected
(Cheng et al., 2017)	0.87 ¹	--	--	--	--	3D patch-level	None detected
(Cheng and Liu, 2017)	0.85 ¹	--	--	--	--	3D subject-level	None detected
(Islam and Zhang, 2018)	--	--	--	--	CN vs mild vs moderate vs severe: 0.93 ^{1†}	2D slice-level	None detected
(Korolev et al., 2017)	0.80 ¹	--	--	--	--	3D subject-level	None detected
(Li et al., 2017)	0.88 ¹	--	--	--	--	3D subject-level	None detected
(Li et al., 2018)	0.90 ¹	--	0.74 ^{1†}	--	--	3D patch-level	None detected
(Lian et al., 2018)	0.90 ¹	0.80 ^{1†}	--	--	--	3D patch-level	None detected
(Mingxia Liu et al., 2018a)	0.91 ¹	0.78 ^{1†}	--	--	--	3D patch-level	None detected
(Mingxia Liu et al., 2018c)	0.91 ¹	--	--	--	--	3D patch-level	None detected
(Qiu et al., 2018)	--	0.83 ^{1†}	--	--	--	2D slice-level	None detected
(Senanayake et al., 2018)	0.76 ¹	--	0.75 ¹	0.76 ¹	--	3D subject-level	None detected
(Shmulev et al., 2018)	--	0.62 ¹	--	--	--	3D subject-level	None detected
(Valliani and Soni, 2017)	0.81 ¹	--	--	--	AD vs MCI vs CN: 0.57 ¹	2D slice-level	None detected

(B) Data leakage Table

Study	Performance					Approach	Data leakage (type)
	AD vs CN	sMCI vs pMCI	MCI vs CN	AD vs MCI	Multi-class		
(Aderghal et al., 2017a)	0.91 ¹	--	0.66 ¹	0.70 ¹	--	ROI-based	Unclear (b,c)
(Basaia et al., 2019)	0.99 ²	0.75 ²	--	--	--	3D subject-level	Unclear (b)
(Hon and Khan, 2017)	0.96 ¹	--	--	--	--	2D slice-level	Unclear (a,c)
(Hosseini Asl et al., 2018)	0.99 ¹	--	0.94 ¹	1.00 ¹	AD vs MCI vs CN: 0.95 ¹	3D subject-level	Unclear (a)
(Islam and Zhang, 2017)	--	--	--	--	CN vs mild vs moderate vs severe: 0.74 ^{1†}	2D slice-level	Unclear (b,c)
(Lin et al., 2018)	0.89 ¹	0.73 ¹	--	--	--	ROI-based	Unclear (b)
(Manhua Liu et al., 2018)	0.85 ¹	0.74 ¹	--	--	--	3D patch-level	Unclear (d)
(Taqi et al., 2018)	1.00 ¹	--	--	--	--	2D slice-level	Unclear (b)
(Vu et al., 2017)	0.85 ¹	--	--	--	--	3D subject-level	Unclear (a)
(S.-H. Wang et al., 2018)	0.98 ¹	--	--	--	--	2D slice-level	Unclear (b)
(Bäckström et al., 2018)*	0.99 ¹	--	--	--	--	3D subject-level	Clear (a)
(Farooq et al., 2017)	--	--	--	--	AD vs LMCI vs EMCI vs CN: 0.99 ^{1†}	2D slice-level	Clear (a,c)
(Gunawardena et al., 2017)	--	--	--	--	AD vs MCI vs CN: 0.96 ¹	3D subject-level	Clear (a,b)
(Vu et al., 2018)	0.86 ¹	--	0.86 ¹	0.77 ¹	AD vs MCI vs CN: 0.80 ¹	3D subject-level	Clear (a,c)
(Wang et al., 2017)	--	--	0.91 ¹	--	--	2D slice-level	Clear (a,c)
(Wang et al., 2019)	0.99 ¹	--	0.98 ¹	0.94 ¹	AD vs MCI vs CN: 0.97 ¹	3D subject-level	Clear (b)
(Wu et al., 2018)	--	--	--	--	sMCI vs pMCI vs CN: 0.95 ^{1†}	2D slice-level	Clear (a,b)

3.2.1. 2D slice-level CNN

Several studies used 2D CNNs with input composed of the set of 2D slices extracted from the MRI 3D volume (Farooq et al., 2017; Gunawardena et al., 2017; Hon and Khan, 2017; Islam and Zhang, 2018, 2017; Qiu et al., 2018; Taqi et al., 2018; Valliani and Soni, 2017; Wang et al., 2017; S.-H. Wang et al., 2018; Wu et al., 2018). The main advantages of this approach are: i) existing CNNs which had huge successes for natural image classification tasks (e.g. ResNet and VGGNet) can be easily borrowed and used in a transfer learning fashion; ii) the number of training samples is the number of slices, thus potentially much larger than the number of subjects.

In this subsection of the bibliography, we found only one study in which neither data leakage was detected neither biased metrics were used (Valliani and Soni, 2017). They used a single axial slice per subject (taken in the middle of the 3D volume) to compare the ResNet to an original CNN with only one convolutional layer and two FC layers. They studied the impact of both transfer learning by initializing their networks with models trained on ImageNet, and data augmentation with affine transformations. They

conclude that the ResNet architecture is more efficient than their baseline CNN and that pre-training and data augmentation improve the accuracy of the ResNet architecture.

In all other studies, we detected a problem in the evaluation: either data leakage was present (or at least suspected) (Farooq et al., 2017; Gunawardena et al., 2017; Hon and Khan, 2017; Islam and Zhang, 2017; Taqi et al., 2018; Wang et al., 2017; S.-H. Wang et al., 2018; Wu et al., 2018) or they used an imbalanced metric on a severely imbalanced dataset (one class is less than half of the other) (Islam and Zhang, 2018; Qiu et al., 2018). Causes of data leakage are described in 3.1 section. These studies differ in terms of slice selection: i) one study used all slices of a given plane (except the very first and last ones that are not informative) (Farooq et al., 2017); ii) other studies selected several slices using an automatic (Hon and Khan, 2017; Wu et al., 2018) or manual criterion (Qiu et al., 2018); iii) one study used only one slice (S.-H. Wang et al., 2018). Working with several slices implies to fuse the classifications obtained at the slice-level to obtain a classification at the subject-level. Only one study (Qiu et al., 2018) explained how they performed this fusion. Other studies didn't implement fusion and reported the slice-level accuracy (Farooq et al., 2017; Gunawardena et al., 2017; Hon and Khan, 2017; Wang et al., 2017; Wu et al., 2018) or it is unclear if the accuracy was computed at the slice- or subject-level (Islam and Zhang, 2018, 2017; Taqi et al., 2018).

The main limitation of the 2D slice-level approach is that MRI is 3-dimensional, whereas the 2D convolutional filters analyze all slices of a subject independently. Moreover, there are many different ways to select slices that are used as input (as all of them may not be informative) and slice-level accuracy and subject-level accuracy are often confused.

3.2.2. 3D patch-level CNN

To compensate for the absence of 3D information in the 2D slice-level approach, more studies focused on the 3D patch-level classification (see Table 1). In these frameworks, the input is composed of a set of 3D patches extracted from an image. In principle, this could result, as in the 2D slice-level approach, in a larger sample size, since the number of samples would be the number of patches (and not the number of subjects). However, this potential advantage is not used in the surveyed papers because they trained independent CNNs for each patch. Additional advantages of patches are the lower memory usage which may be useful when one has limited resources and the lower number of learnt parameters. However, this last advantage is present only when one uses the same network for all patches.

Two studies (Cheng et al., 2017; Manhua Liu et al., 2018) used very large patches. Specifically, they extracted 27 overlapping 3D patches of size 50x41x40 voxels covering the whole volume of the MRI data (100x81x80 voxels). They individually trained 27 convolutional networks (one per patch) comprising four convolutional layers and two FC layers. Then, an ensemble CNN was trained to provide a decision at the subject level. This ensemble CNN is partly initialized with the weights of the previously trained CNNs. (Manhua Liu et al., 2018) reused exactly the same architecture than (Cheng et al., 2017) and enriched it with a fusion of PET and MRI inputs. They also gave the results obtained using the MRI modality only, which is the result reported in Table 1.

(Li et al., 2018) used smaller patches (32x32x32). By decreasing the size of the patches, they had to take into account a possible discrepancy between patches taken at the same coordinates for different subjects. To avoid this dissimilarity between subjects without performing a non-linear registration, they clustered their patches using k-means. Then they trained one CNN per cluster, and assembled the features obtained at the cluster-level in a similar way than (Cheng et al., 2017; Manhua Liu et al., 2018).

The following three studies (Lian et al., 2018; Mingxia Liu et al., 2018a, 2018c) decided to use even smaller patches (19x19x19). Nevertheless, they did not use all possible patches from the MRI data but chose only some of them based on anatomical landmarks. These anatomical landmarks are found in a supervised manner via a group comparison between AD and CN subjects. However, this method requires a non-linear registration in order to build the correspondence between voxels of different subjects. Similarly to other studies, in (Mingxia Liu et al., 2018c), one CNN is pre-trained for each patch and the outputs are fused to obtain the diagnosis of a subject. The approach of (Mingxia Liu et al., 2018a) is slightly different as they consider that one patch cannot be labelled with a diagnosis, hence they do not train one CNN per patch

individually before ensemble learning but train the ensemble network from scratch. Finally (Lian et al., 2018) proposed a weakly-supervised guidance: the loss of the network is based on the final classification scores at the subject-level as well as the intermediate classification done on the patch- and region-level.

There are far less data leakage problems in this section, with only one doubt on the validity of the transfer learning between the AD vs CN task and the MCI vs CN task in (Manhua Liu et al., 2018) because of a lack of explanations. Nevertheless this has no impact on the result of the AD vs CN task for which we didn't detect any problem of data leakage.

As for 2D-slice level in which a selection of slices must be made, one must choose the size and stride of patches. The choice of these hyperparameters will depend on the MRI preprocessing (e.g. a non-linear registration is likely needed for smaller patches). Nevertheless, note that the impact of these hyperparameters has been studied in the pre-cited studies (which has not been done for the 2D slice-level approaches). The main drawback of these approaches is the complexity of the framework: one network is trained for each patch position and these networks are successively fused and retrained at different levels of representation (region-level, subject-level).

3.2.3. ROI-based CNN

3D patch-level methods use the whole MRI by slicing it in smaller inputs. However, most of these patches are not informative as they contain parts of the brain that are not affected by the disease. Methods based on regions of interest (ROI) overcome this issue by focusing on regions which are known to be informative. In this way, the complexity of the framework can be decreased as fewer inputs are used to train the networks. In all the following studies, the ROI chosen was the hippocampus, which is well-known to be affected early in AD (Dickerson et al., 2001; Salvatore et al., 2015; Schuff et al., 2009). Studies differ by the definition of the hippocampal ROI.

(Aderghal et al., 2018, 2017a, 2017b) performed a linear registration and defined a 3D bounding box comprising all the voxels of the hippocampus according to a segmentation with the AAL atlas. These three studies used a “2D+ ϵ approach” with patches made of three neighbouring 2D slices in the hippocampus. As they use only one or three patches per patient, they do not cover the entire region. The first study (Aderghal et al., 2017b) only uses the sagittal view and classifies one patch per patient. The architecture of the CNN is made of two convolutional layers associated with max pooling, and one FC layer. In the second study (Aderghal et al., 2017a), all the views (sagittal, coronal and axial) are used to generate patches. Then, three patches are generated per subject and accordingly three networks are trained for each view and then fused. The last study of the same author (Aderghal et al., 2018) focuses on the transfer learning from anatomical MRI to diffusion MRI, which is out of our scope.

In (Lin et al., 2018) a non-linear registration was performed to obtain a voxel correspondence between the subjects, and the voxels belonging to the hippocampus¹² were identified after a segmentation implemented with MALP-EM (Ledig et al., 2015). 151 patches were extracted per image with sampling positions fixed during experiments. Each of them was made of the concatenation of three 2D slices along the three possible planes (sagittal, coronal and axial) originated at one voxel belonging to the hippocampus.

The main drawback of this methodology is that it studies only one (or a few) regions while AD alterations span over multiple brain areas. However, it may allow to avoid overfitting because the inputs are smaller (~3000 voxels in our bibliography) and fewer than in methods allowing patch combinations.

3.2.4. 3D subject-level CNN

Recently, with the boost of high-performance computing resources, more studies used a 3D subject-level approach (see Table 1). In this approach, the whole MRI is used at once and the classification is performed at the subject level. The advantage is that the spatial information is fully integrated.

¹² In their original paper, this anatomical structure was called the “hippopotamus” (sic).

Some studies readapted two classical architectures to fit the whole MRI: the ResNet and VGGNet (Korolev et al., 2017; Shmulev et al., 2018). In both cases, results obtained on VGG and ResNet are equivalent, and their best results are below those of other studies of the same section. Another study (Senanayake et al., 2018) proposed to use a set of complex modules from classical architectures such as ResNet and DenseNet (dilated convolutions, dense blocks and residual blocks), also without success.

Other studies defined original architectures (Bäckström et al., 2018; Basaia et al., 2019; Cheng and Liu, 2017; Hosseini Asl et al., 2018; Li et al., 2017; Vu et al., 2018, 2017; Wang et al., 2019). Among these, we did not detect data leakage in only three of them (Bäckström et al., 2018; Cheng and Liu, 2017; Li et al., 2017). (Bäckström et al., 2018; Cheng and Liu, 2017) had a similar approach by training one network from scratch on augmented data. One crucial difference between these two studies is the preprocessing step: (Bäckström et al., 2018) used a non-linear registration whereas (Cheng and Liu, 2017) performed no registration. (Li et al., 2017) proposed a more complex framework fusing the results of a CNN and three networks pre-trained with an AE.

For the other studies using original architectures, we suspect data leakage (Bäckström et al., 2018; Basaia et al., 2019; Hosseini Asl et al., 2018; Vu et al., 2018, 2017; Wang et al., 2019), hence their performance cannot be fairly compared to the previous ones. However we noted that (Hosseini Asl et al., 2018; Vu et al., 2018, 2017) studied the impact of pre-training with an AE, and concluded that it improved their results (accuracy increased from 5 to 10 percent points).

In 3D-subject level approach the number of samples is small compared to the number of parameters to optimize. Indeed, there is one sample per subject, typically a few hundreds to thousands subjects in a dataset, thus increasing the risk of overfitting.

3.2.5. Conclusion

A high number of these 32 studies presented biased performance because of data leakage: 10 were labeled as *Unclear* because of lack of explanations, and 6 as *Clear* in which we assert the presence of data leakage (we do not count here the study of Backstrom et al (Bäckström et al., 2018) as data leakage was done deliberately to study its impact). This means that about 50% of the surveyed studies could report biased performances (see Table 1 and Section 3.1 for more details).

In addition to that problem, most studies are not comparable because the datasets used, subjects selected among them and preprocessing performed are different. Furthermore, these studies often do not motivate the choice of their architecture or hyperparameters. It might be that many of them have been tried (but not reported) thereby resulting in biased performances on the test set. Finally, the code is often not available, neither are key implementation details (such as hyperparameters values) making them difficult if not impossible to reproduce.

3.3. Other deep learning approaches for AD classification

Several studies found in our literature search are out of our scope: either CNNs were not used in an end-to-end manner or not applied to images, or other network architectures were implemented, or the approach required longitudinal or multimodal data.

In several studies, the CNN is used as a feature extractor only and the classification is performed using either a random forest (Chaddad et al., 2018), SVM with linear or polynomial kernels and logistic regression (Çitak-ER et al., 2017), extreme ML (Lin et al., 2018), SVM with different kernels (Shen et al., 2018), or logistic regression and XGBoost (decision trees) (Shmulev et al., 2018). Only Shmulev et al compared the results obtained with the CNN classification and those obtained with other classifiers based on features extracted by the CNN and concluded that the latter is more efficient. Instead of being directly applied to the image, CNNs can be applied to pre-extracted features. This is the case of (Suk et al., 2017) where the CNN is applied to the outputs of several regression models performed between MRI-based features and

clinical scores with different hyperparameters. CNNs can also be applied to non-Euclidean spaces, such as graphs of patients (Parisot et al., 2018) or the cortical surface (Mostapha et al., 2018).

Other architectures have been applied to anatomical MRI. Many studies used a variant of the multilayer perceptron composed of stacked FC layers (Amoroso et al., 2018; Baskar et al., 2018; Cárdenas-Peña et al., 2017, 2016; Dolph et al., 2017; Gorji and Haddadnia, 2015; Gutiérrez-Becker and Wachinger, 2018; Jha et al., 2017; Lu et al., 2018; Mahanand et al., 2012; Maitra and Chatterjee, 2006; Ning et al., 2018; Raut and Dalal, 2017; Shams-Baboli and Ezoji, 2017; Zhang et al., 2018; Zhou et al., 2019) or of a probabilistic neural network (Duraismy et al., 2019; Mathew et al., 2018). In other studies, high-level representations of the features are extracted using both unsupervised (deep Boltzmann machine (Suk et al., 2014) and AE (Suk et al., 2015)) and supervised structures (deep polynomial networks (Shi et al., 2018)), and an SVM is used for classification. Non-CNNs architectures require extensive preprocessing as they have to be applied to imaging features such as cortical thickness, shapes, or texture and regional features. Moreover, feature selection or embedding is also often required (Amoroso et al., 2018; Dolph et al., 2017; Jha et al., 2017; Lu et al., 2018; Mahanand et al., 2012; Mathew et al., 2018; Suk et al., 2015, 2014) to further reduce dimensionality.

DL-based classification approaches are not limited to cross-sectional anatomical MRI. Longitudinal studies exploit information extracted from several time points of the same subject. A specific structure, the recurrent neural network, has been used to study the temporal correlation between the images (Bhagwat et al., 2018; Cui et al., 2018; X. Wang et al., 2018). Several studies exploit multi-modal data (Aderghal et al., 2018; Cheng and Liu, 2017; Esmailzadeh et al., 2018; Li et al., 2015; Liu et al., 2016, 2015; Manhua Liu et al., 2018; Mingxia Liu et al., 2018b; Lu et al., 2018; Ning et al., 2018; Ortiz et al., 2016; Qiu et al., 2018; Raut and Dalal, 2017; Senanayake et al., 2018; Shi et al., 2018; Shmulev et al., 2018; Spasov et al., 2018; Suk et al., 2014; Thung et al., 2017; Vu et al., 2018, 2017; Zhou et al., 2019, 2017), such as multiple imaging modalities (positron emission tomography and diffusion tensor imaging), demographic data, genetics, clinical scores, or cerebrospinal fluid biomarkers. Note that multimodal studies that also reported results with MRI only (Aderghal et al., 2018; Cheng and Liu, 2017; Manhua Liu et al., 2018; Qiu et al., 2018; Senanayake et al., 2018; Shmulev et al., 2018; Vu et al., 2018, 2017) are displayed in Table 1. Exploiting multiple time-points and/or modalities is expected to improve the classification performance. However, these studies can be limited by the small number subjects having all the required time points and modalities.

4. Materials

The data used in our study are from three public datasets: ADNI AIBL and OASIS. Information about these datasets is presented in supplementary eMethod 2. We used the T1w MRI available in each of these studies. For the detailed MRI protocols, one can see (Samper-González et al., 2018). This also describes which T1 MRI was chosen in case where multiple images for a given visit exist.

The ADNI dataset used in our experiments comprises 1455 participants for whom a T1w MR image was available at at least one visit. For each ADNI subset, five diagnosis groups were considered:

- CN: sessions of subjects who were diagnosed as CN at baseline and stayed stable during the follow-up;
- AD: sessions of subjects who were diagnosed as AD at baseline and stayed stable during the follow-up;
- MCI: sessions of subjects who were diagnosed as MCI, EMCI or LMCI at baseline, who did not encounter multiple reversions and conversions and who did not regress to CN diagnosis;
- pMCI: sessions of subjects who were diagnosed as MCI, EMCI or LMCI at baseline, and progressed to AD between the current visit and the visit at 36 months;
- sMCI: sessions of subjects who were diagnosed as MCI, EMCI or LMCI at baseline, never progressed to AD months and were followed at least 36 months after the current visit.

Naturally, all sessions of the pMCI and sMCI groups are included in the MCI group. Note that the reverse is false, as some MCI subjects did not convert to AD but were not followed long enough to state whether they were sMCI. Moreover, for 30 sessions, the preprocessing did not pass the quality check (QC) (see the Method section) and these data were removed from our dataset. 2 subjects were entirely removed because the preprocessing failed for all their sessions. Table 2 summarizes the demographics, and the MMSE and global CDR scores of the ADNI participants.

Table 2. Summary of participant demographics, mini-mental state examination (MMSE) and global clinical dementia rating (CDR) scores for ADNI.

	Subjects	Sessions	Age	Gender	MMSE	CDR
CN	330	1 830	74.4 ± 5.8 [59.8, 89.6]	160 M / 170 F	29.1 ± 1.1 [24, 30]	0: 330
MCI	787	3 458	73.3 ± 7.5 [54.4, 91.4]	464 M / 323 F	27.5 ± 1.8 [23, 30]	0: 2; 0.5: 785
sMCI	298	1 046	72.3 ± 7.4 [55.0, 88.4]	175 M / 123 F	28.0 ± 1.7 [23, 30]	0.5: 298
pMCI	295	865	73.8 ± 6.9 [55.1, 88.3]	176 M / 119 F	26.9 ± 1.7 [23, 30]	0.5: 293; 1: 2
AD	336	1 106	75.0 ± 7.8 [55.1, 90.9]	185 M / 151 F	23.2 ± 2.1 [18, 27]	0.5: 160; 1: 175; 2: 1

Values are presented as mean ± SD [range]. M: male, F: female

The AIBL dataset considered in this work is composed of 598 participants for whom a T1w MR image and an age value was available at at least one visit. The criteria used to create the diagnosis groups are identical to the ones used for ADNI. Table 3 summarizes the demographics, and the MMSE and global CDR scores of the AIBL participants. After the preprocessing pipeline, 7 sessions were removed without changing the number of subjects.

Table 3. Summary of participant demographics, mini-mental state examination (MMSE) and global clinical dementia rating (CDR) scores for AIBL.

	N	Age	Gender	MMSE	CDR
CN	429	72.5 ± 6.2 [60, 92]	183 M / 246 F	28.8 ± 1.2 [25, 30]	0: 406; 0.5: 22; 1: 1
MCI	93	75.4 ± 6.9 [60, 96]	50 M / 43 F	27.0 ± 2.1 [20, 30]	0: 6; 0.5: 86; 1: 1
sMCI	13	76.7 ± 6.5 [64, 87]	8 M / 5 F	28.2 ± 1.5 [26, 30]	0.5: 13
pMCI	20	78.1 ± 6.6 [63, 91]	10 M / 10 F	26.7 ± 2.1 [22, 30]	0.5: 20
AD	76	73.9 ± 8.0 [55, 93]	33 M / 43 F	20.6 ± 5.5 [6, 29]	0.5: 31; 1: 36; 2: 7; 3: 2

Values are presented as mean ± SD [range]. M: male, F: female

The OASIS dataset considered in this work is composed of 193 participants aged 62 years or more (minimum age of the participants diagnosed with AD). Table 4 summarizes the demographics, and the MMSE and global CDR scores of the OASIS participants. After the preprocessing pipeline, 39 sessions were excluded leading to the loss of the same amount of subjects.

Table 4. Summary of participant demographics, mini-mental state examination (MMSE) and global clinical dementia rating (CDR) scores for OASIS.

	N	Age	Gender	MMSE	CDR
CN	76	76.5 ± 8.4 [62, 94]	14 M / 62 F	29.0 ± 1.2 [25, 30]	0: 76
AD	78	75.6 ± 7.0 [62, 96]	35 M / 43 F	24.4 ± 4.3 [14, 30]	0.5: 56; 1: 20; 2: 2

Values are presented as mean ± SD [range]. M: male, F: female

5. Methods

In this section, we present the main components of our framework: automatic converters of public datasets for reproducible data management (Section 5.1), preprocessing of MRI data (5.2), classification models (5.3), transfer learning approaches (5.4), classification tasks (5.5), evaluation strategy (5.6) and framework implementation details (5.7).

5.1. Converting datasets to a standardized data structure

ADNI, AIBL and OASIS, as public datasets, are extremely useful to the research community. However, they may be difficult to use because the downloaded raw data do not possess a clear and uniform organization. We thus used our previously developed converters (Samper-González et al., 2018) (available in the open source software platform Clinica) to convert the raw data into the BIDS format (Gorgolewski et al., 2016). Finally, we organized all the outputs of the experiments into a standardized structure, inspired from BIDS.

5.2. Preprocessing of T1w MRI

In principle, CNN require only minimal preprocessing because of their ability to automatically extract low-to-high level features. However, in AD classification where datasets are relatively small and thus where deep networks may be difficult to train, it remains unclear whether they can benefit from more extensive preprocessing. Moreover, previous studies have used varied amounts of preprocessing procedures but without systematically assessing their impact. Thus, in the current study, we compared two different image preprocessing procedures: one “Minimal” and one more “Extensive” procedure. Both procedures included bias correction, and (optional) intensity rescaling. In addition, the “Minimal” processing included a linear registration while the “Extensive” included non-linear registration and skull-stripping.

In brief, the “Minimal” preprocessing procedure performs the following operations. The N4ITK method (Tustison et al., 2010) was firstly used to correct the bias field. Next, a linear (affine) registration was performed using SyN algorithm from ANTs (Avants et al., 2008) to register each image from the native space to the MNI space (ICBM 2009c nonlinear symmetric template) (Fonov et al., 2011, 2009). To improve the computational efficiency, the registered images were further cropped to remove the border background. The final image size is $169 \times 208 \times 179$ with 1 mm^3 isotropic voxels. Intensity rescaling, which was performed based on the min and max values, denoted as MinMax, was set to be optional to study its influence on classification results.

In the “Extensive” preprocessing procedure, bias correction and non-linear registration are performed using the Unified Segmentation approach (Ashburner and Friston, 2005) available in SPM12¹³. Note that we do not use the tissue segmentation but only the nonlinearly registered, bias corrected, MR images. Subsequently, we perform skull-stripping based on a brain mask drawn in MNI space. We chose this mask-based approach over direct image-based skull-stripping procedures because the later did not prove robust on our data. This mask-based approach is less accurate but more robust. In addition, we performed intensity rescaling as in the “Minimal” pipeline.

We performed QC on the outputs of the preprocessing procedures. For the “Minimal” procedure, we used DL-based QC framework¹⁴ (Fonov et al., 2018) to automatically check the quality of the linearly registered data. This software outputs a probability indicating how accurate the registration is. We visually checked the scans whose probability was lower than a threshold of 0.70. Out of these, 30 ADNI scans, 7 AIBL scans, and 39 OASIS scans had a bad linear registration and were excluded.

¹³<http://www.fil.ion.ucl.ac.uk/spm/software/spm12/>

¹⁴ <https://github.com/vfonov/deep-qc>

5.3. Classification models

We considered four different approaches for classification: i) 3D subject-level CNN, ii) 3D ROI-based CNN, iii) 3D patch-level CNN and iv) 2D slice-level CNN.

In the case of DL, one challenge is to find the “optimal” model (i.e. global minima), including the architecture hyperparameters (e.g. number of layers, dropout, batch normalization) and the training hyperparameters (e.g. learning rate, weight decay).

We first reviewed the architectures used in the literature among the studies in which no data leakage problem was witnessed (Table 1A). There was no consensus in the literature, thus we used the following heuristic strategy for the each of the four approaches.

For the 3D subject-level approach, we began with an overfitting model that was very heavy because of the high number of FC layers (4 convolutional blocks + 5 FC layers). Then, we iteratively repeated the following operations:

- the number of FC layers was decreased until accuracy on the validation set decreased substantially;
- we added one more convolutional block.

In this way, we explored the architecture space from 4 convolutional blocks + 5 FC layers to 7 convolutional blocks + 2 FC layers. Among the best performing architectures, we chose the shallowest one: 5 convolutional blocks + 3 FC layers.

As the performance was very similar for the different architectures tested with the 3D subject-level approach and as this search method is time costly, it was not used for the 3D patch-level approach for which only four different architectures were tested:

- 4 convolutional blocks + 2 FC layers
- 4 convolutional blocks + 1 FC layer
- 7 convolutional blocks + 2 FC layers
- 7 convolutional blocks + 1 FC layer

The best architecture (4 convolutional blocks + 2 FC layers) was kept and used both in 3D patch-level and ROI-based approaches. Note that the other architectures were only slightly worse.

For these 3 approaches, other architecture hyperparameters were explored: with or without batch normalization, with or without dropout.

For the 2D slice-level approach, we chose to use a classical architecture, the ResNet-18 with FC layers added at the end of the network. We explored from 1 to 3 added FC layers and the best results were obtained with one. We then explored the number of layers to fine-tune (2 FC layers or the last residual block + 2 FC layers) and chose to fine-tune the last block and the 2 FC layers. We always used dropout and tried different dropout rates.

For all four approaches, training hyperparameters (learning rate, weight decay) were adapted for each model depending on the evolution of the training accuracy.

The list of the chosen architecture hyperparameters is given in online supplementary eTables 1, 2 and 3. The list of the chosen training hyperparameters is given in online supplementary eTables 4 and 5.

5.3.1. 3D subject-level CNN

For the 3D-subject-level approach, the proposed CNN architecture is shown in Figure 2. The CNN consisted of 5 convolutional blocks, 3 FC layers and one softmax layer. Each convolutional block was sequentially made of one convolutional layer, one batch normalization layer, one ReLU and one max pooling layer (more architecture details are provided in online supplementary eTable 1).

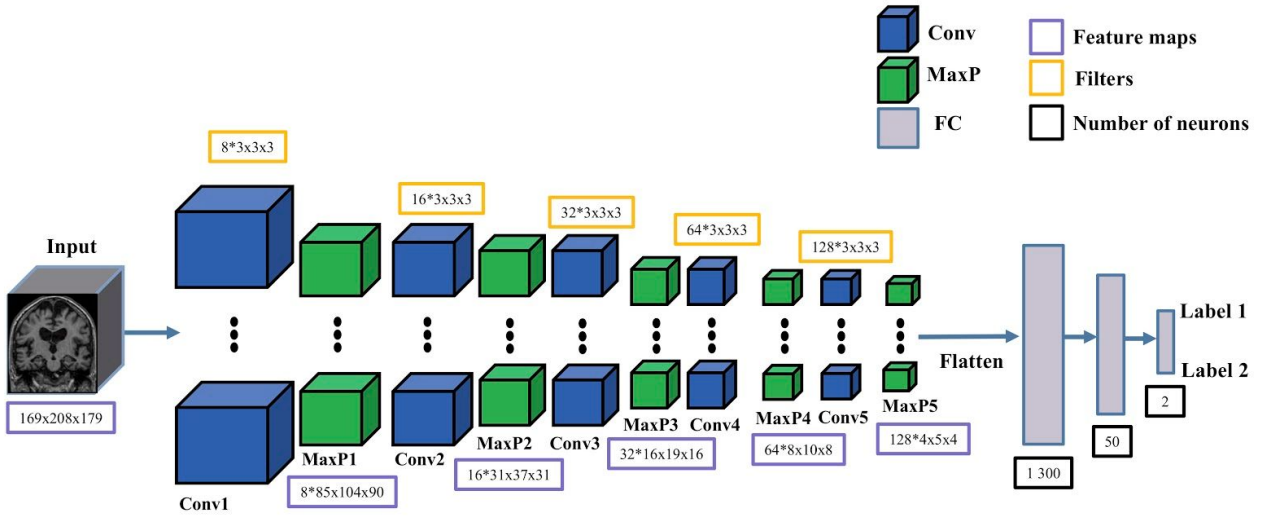


Figure 2: Architecture of the 3D subject-level CNNs. For each convolutional block, we only presented the convolutional layer and max pooling layer. Filters for each convolutional layer represent the number of filters \times filter size. Feature maps of each convolutional block represent the number of feature maps \times size of each feature map. Conv: convolutional layer; MaxP: max pooling layer; FC: fully connected layer.

5.3.2. 3D ROI-based and 3D patch-level CNN

For the 3D ROI-based and 3D patch-level approaches, the chosen CNN architecture, shown in Figure 3, consisted of 4 convolutional blocks (with the same structure as in the 3D subject-level), 3 FC layers and one softmax layer (more architecture details are provided in online supplementary eTable 2).

To extract the 3D patches, a sliding window ($50 \times 50 \times 50 \text{ mm}^3$) without overlap was used to convolve over the entire image, generating 36 patches for each image.

For the 3D ROI-based approach, we chose the hippocampus as a ROI, as done in previous studies. We used a cubic patch ($50 \times 50 \times 50 \text{ mm}^3$) enclosing the left (resp. right) hippocampus. The center of this cubic patch was manually chosen based on the MNI template image (ICBM 2009c nonlinear symmetric template). We ensured visually that this cubic patch included all the hippocampus.

For the 3D patch-level approach, two different training strategies were considered. First, all extracted patches were fitted into a single CNN (denoting this approach as 3D patch-level single-CNN). Secondly, we used one CNN for each patch, resulting in finally 36 (number of patches) CNNs (denoting this approach as 3D patch-level multi-CNN).

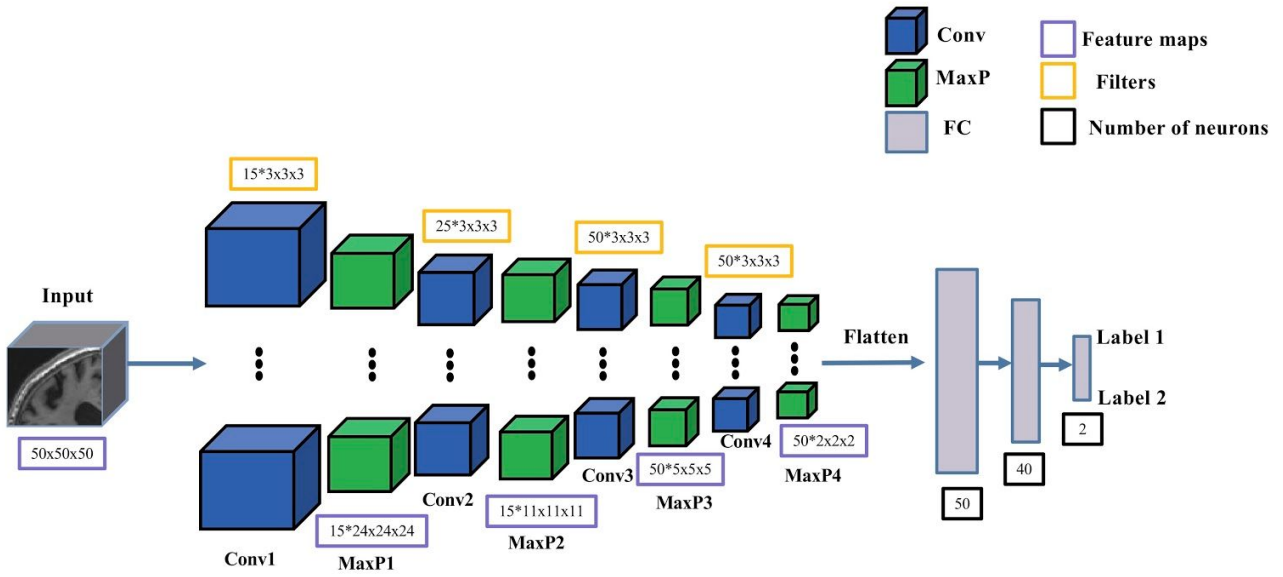


Figure 3: Architecture of the 3D ROI-based and 3D patch-level CNNs. For each convolutional block, we only presented the convolutional layer and max pooling layer. Filters for each convolutional layer represent the number of filters \times filter size. Feature maps of each convolutional block represent the number of feature maps \times size of each feature map. Conv: convolutional layer; MaxP: max pooling layer; FC: fully connected layer.

5.3.3. 2D slice-level CNN

For 2D slice-level, the ResNet pre-trained on ImageNet was adopted and fine-tuned. The architecture is shown in Figure 4. The architecture details of ResNet can be found in He et al (He et al., 2016). We added one FC layer and one softmax layer on top of the ResNet (more architecture details are provided in online supplementary eTable 3). Fine-tuning was performed only on the last convolutional layers and last FC layer and the added FC layer. The weight and bias of the other layers of the CNN were frozen during fine-tuning to avoid overfitting.

For each subject, each sagittal slice was extracted and replicated into R, G and B channels respectively, in order to generate a RGB image. The first and last twenty slices were excluded due to the lack of information, which resulted in 129 RGB slices for each image.

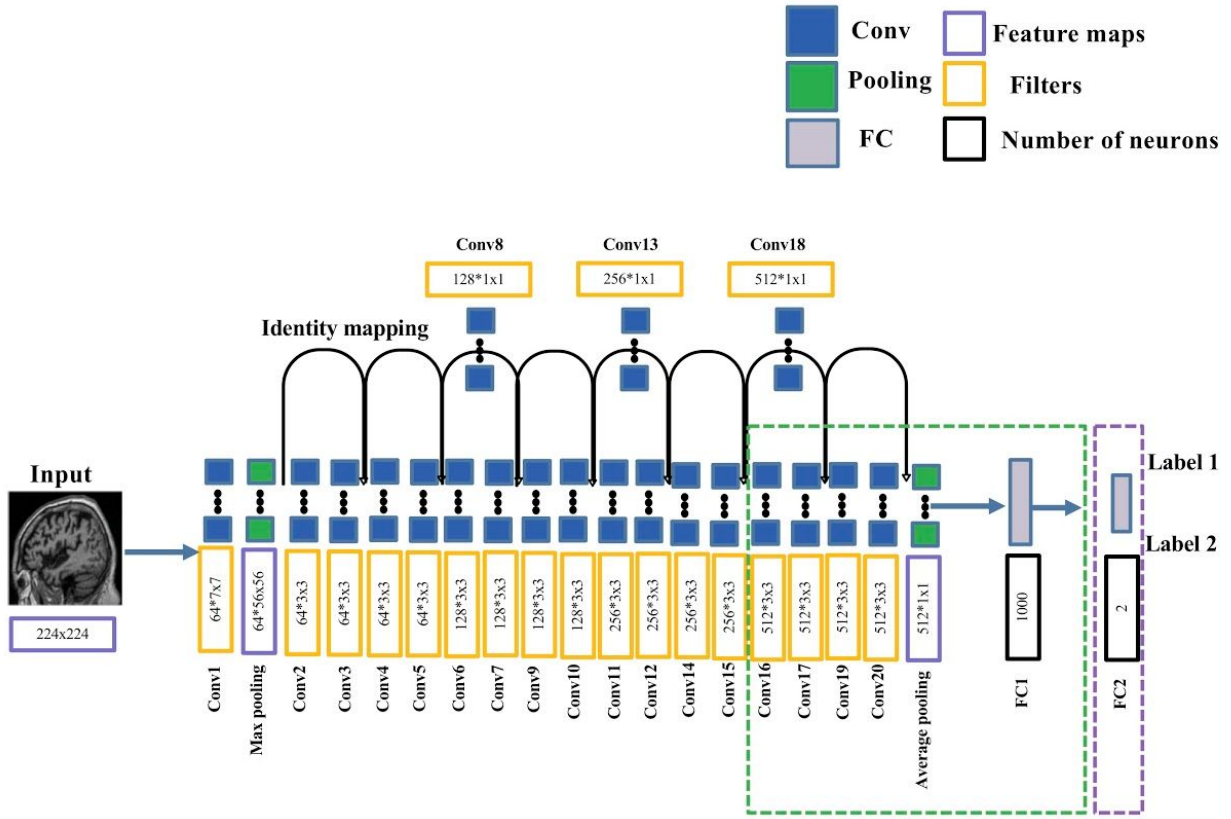


Figure 4: Architecture of the 2D slice-level CNN. An FC layer (FC2) was added on top of the ResNet. The last five convolutional layers and the last FC of ResNet (green dotted box) and the added FC layer (purple dotted box) were fine-tuned and the other layers were frozen during training. Filters for each convolutional layer represent the number of filters \times filter size. Feature maps of each convolutional block represent the number of feature maps \times size of each feature map. Conv: convolutional layer; FC: fully connected layer.

5.3.4. Majority voting system

For 3D patch-level, 3D ROI-based and 2D slice-level CNNs, we adopted a soft voting system (Raschka, 2015) to generate the subject-level decision. The subject-level decision is generated based on the decision for each slice (resp. for each patch / for the left and right hippocampus ROI).

The subject-level decision was calculated based on the predicted probabilities p of all the slices/patches/ROIs/CNNs from the same patient:

$$\hat{y} = \arg \max_i \sum_j^m w_j p_{ij}$$

where w_j is the weight assigned to the j -th patch/slice/ROI/CNN. w_j reflects the importance of each slice/patch/ROI/CNN and is weighted by the normalized accuracy of the j -th slice/patch/ROI/CNN.

For 3D patch-level multi-CNN approach, the 36 CNNs were trained independently. In this case, the weaker classifiers' weight (accuracy < 0.7) was set to be 0 with the consideration that the labels' probabilities of these classifiers could harm the majority voting system (e.g. AD and CN has both probabilities near to 0.5).

5.3.5. Comparison to a linear SVM on voxel-based features

For comparison purpose, classification was also performed with a linear SVM classifier. The SVM took as input the modulated GM density maps non-linearly registered using the DARTEL method (Ashburner, 2007) as in our previous study (Samper-González et al., 2018).

5.4. Transfer learning

Two different approaches were used for transfer learning: i) AE pre-training for 3D CNNs; and ii) ResNet pre-trained on ImageNet for 2D CNNs.

5.4.1. AE pre-training

The AE was constructed based on the corresponding architecture of CNN. Specifically, the encoder part of the AE shared the same architecture with the CNN: the encoder is composed of a sequence of convolutional blocks, each block having one convolutional layer, one batch normalization layer, one ReLU and one max pooling layer. The architecture of the decoder mirrored that of the encoder, except that the order of the convolution layer and the ReLU was swapped. Of note, the pre-training with AE and classification with CNNs in our experiments used the same training and validation data splits in order to avoid potential data leakage problems. Also, each AE was trained on all available data in the training sets. For instance, all MCI, AD and CN subjects in training dataset were used to pre-train the AE for the AD vs CN classification task.

5.4.2. ImageNet pre-training

For the 2D-slice experiments, we investigated the possibility to transfer a ResNet pre-trained on ImageNet (He et al., 2016) to our specific tasks. Next, the fine-tuning procedure was performed on the chosen layers (see Figure 4).

5.5. Classification tasks

We performed two tasks in our application: first, the AD vs CN classification, a baseline task to easily compare the results of our different framework. Then the best frameworks obtained on this task were selected to perform the prediction task sMCI vs pMCI: the weights and biases of the model learnt on the source task (AD vs CN) were transferred to a new model fine-tuned on the target task (sMCI vs pMCI). For SVM, the sMCI vs pMCI was done either training directly on sMCI vs pMCI or using training on AD vs CN and applying the trained model to sMCI vs pMCI.

5.6. Evaluation strategy

5.6.1. Validation procedure

Rigorous validation is essential to objectively assess the performance. This is particularly critical in the case of DL as one may easily overfit the validation dataset when manually performing model selection and hyperparameter fine-tuning. An independent test set should be, at the very beginning, partitioned and concealed. It should not be touched until the CV, based on the training and validation dataset, is finished and the final model is chosen. This test dataset should be used only to assess the performance (i.e. generalization) of a fully specified and trained classifier (Kriegeskorte et al., 2009; Ripley, 1996; Sarle, 1997). Considering this, we chose a classical split into training/validation/test sets. Training/validation sets were used in a CV procedure for model selection while the test set was left untouched. Of note, as mentioned in the beginning, we have not yet used the test set and will do so only after the review process of the paper has been finished. Only the best performing model for each approach (3D subject-level, 3D patch-level, 3D ROI-based, 2D slice-level) as defined by the CV on training/validation sets, will be tested on the test set.

First, the test set was built as follows. ADNI data was split into training/validation and test sets. The ADNI test dataset consisted of 100 randomly chosen age- and sex-matched subjects for each diagnostic class (i.e. 100 CN subjects, 100 AD patients). The rest of ADNI data was used as training/validation set. We ensured that age and sex distributions between training/validation and test sets were not significantly different. Two other test sets were composed of all subjects of OASIS and AIBL. Thus, as a result, we have three test sets: i) an ADNI test set which will be used to assess model generalization within the same dataset (thereby

assessing that model choice has not overfitted the training/validation set); ii) an AIBL test set which will be used to assess generalization to another dataset but with similar inclusion criteria and image acquisition parameters to those of ADNI; iii) an OASIS test which will be used to assess generalization to other inclusion criteria and image acquisition parameters.

Secondly, the model selection procedure, including model architecture selection and training hyperparameters fine-tuning, was performed using only the training/validation dataset. For that purpose, a 5-fold CV was performed, which resulted in one fold (20%) of the data for validation and the rest for training. Note that the 5-fold data split was performed only once for all experiments with a fixed seed number (*random_state* = 2), thus guaranteeing that all the experiments used exactly the same subjects during CV. Also, no overlapping exists between the MCI subjects used for AE pre-training (using all available AD, CN and MCI) and the test dataset of sMCI vs pMCI. Thus, the evaluation of the cross-task transfer learning (from AD vs CN to sMCI vs pMCI) is unbiased. Finally, for the linear SVM, the hyperparameter C controlling the amount of regularization was chosen using an inner loop of 10-fold CV (thereby performing a nested CV).

5.6.2. Metrics

We computed the following performance metrics: balanced accuracy, AUC, accuracy, sensitivity and specificity. In the manuscript, for the sake of concision, we report only the balanced accuracy but all other metrics are available at <https://gitlab.icm-institute.org/aramislab/AD-ML>.

5.7. Implementation details

The image preprocessing procedures were implemented with Nipype (Gorgolewski et al., 2011). The DL models were built using the Pytorch library¹⁵ (Paszke et al., 2017). The linear SVM was built using scikit-learn (Pedregosa et al., 2011). TensorboardX¹⁶ was embedded into the current framework to dynamically monitor the training process. Specifically, we evaluated and reported the training and validation accuracy/loss after each epoch or certain iterations. Of note, instead of using only the current batch of data, the accuracy was evaluated based on all the training/validation data. Moreover, we organized the classification outputs in a hierarchical way inspired from BIDS, including the TSV files containing the classification results, the outputs of TensorboardX for dynamic monitoring of the training and the best performing models selected based on the validation accuracy.

We applied the following early stopping strategy for all the classification experiments: the training procedure does not stop until the validation loss is continuously higher than the lowest validation loss for N epochs. Otherwise, the training continues to the end of the pre-defined number of epochs. The selected model was the one which obtained the highest validation accuracy during training. For the AE pre-training, the AE was trained to the end of the pre-defined number of epochs. We then visually check the validation loss and the quality of the reconstructed images.

All experiments were performed on the cluster of the Brain and Spine Institute¹⁷ in Paris, which is equipped with 4 NVIDIA P100 GPU cards (64 GB shared memory) and 24 CPUs (120 GB shared memory).

¹⁵ <https://pytorch.org/>

¹⁶ <https://github.com/lanpa/tensorboardX>

¹⁷ <https://icm-institute.org/>

6. Experiments and results

6.1. Results on training/validation set

The different classification experiments and results (validation accuracy during 5-fold CV) are detailed in Table 5. For each experiment, the training process of the best fold (with highest validation accuracy) is presented as illustration (see supplementary eFigures 1-4 for details). Lastly, the training hyperparameters (e.g. learning rate and batch size) for each experiments are presented in supplementary eTable 4.

6.1.1. 3D subject-level

Influence of intensity rescaling. We first assessed the influence of intensity rescaling. Without rescaling, the CNN did not perform better than chance (balanced accuracy = 0.50 ± 0.00) and there was an obvious generalization gap (high training but low validation accuracy). With intensity rescaling, the balanced accuracy improved to 0.77 ± 0.08 . Based on these results, intensity rescaling was used in all subsequent experiments.

Influence of transfer learning (AE pre-training). The performance was slightly higher with AE pre-training (0.78 ± 0.05) than without (0.77 ± 0.08) and the standard deviation was lower. Based on this, we decided to always use AE pre-training, even though the difference is small.

Influence of the training dataset size. We then assessed the influence of the amount of training data, comparing training using only baseline data to those with longitudinal data. The performance was substantially higher with longitudinal data (0.85 ± 0.03) compared to baseline data only (0.78 ± 0.05). We choose to continue exploring the influence of this choice because the four different approaches have a very different number of learnt parameters and the sample size is intrinsically augmented in 2D slice-level and 3D single-CNN patch-level approaches.

Influence of preprocessing. We then assessed the influence of the preprocessing comparing the “Extensive” and “Minimal” preprocessing procedures. The performance was equivalent with the “Minimal” preprocessing (0.85 ± 0.03) and with the “Extensive” preprocessing (0.85 ± 0.05). Hence in the following experiments we kept the “Minimal” preprocessing.

Classification of sMCI vs pMCI. The balanced accuracy was the same for baseline data and for longitudinal data (0.74 ± 0.03).

6.1.2. 3D ROI-based

For AD vs CN, the balanced accuracy was 0.86 ± 0.03 for baseline data and 0.85 ± 0.02 for longitudinal data. This is comparable to the results obtained with the subject-level approach. For sMCI vs pMCI, the balanced accuracy was 0.80 ± 0.03 for baseline data and 0.79 ± 0.03 for longitudinal data. This is substantially higher than with the 3D-subject level approach.

6.1.3. 3D patch-level

Single CNN. The accuracy was 0.72 ± 0.09 for baseline data and 0.72 ± 0.06 for longitudinal data.

Multi CNN. For AD vs CN, the accuracy was 0.81 ± 0.03 for baseline data and 0.79 ± 0.02 for longitudinal data, thereby outperforming the single CNN approach. For sMCI vs pMCI, the accuracy was 0.76 ± 0.04 for baseline data and 0.76 ± 0.03 for longitudinal data. The performance for both tasks is lower than that of the 3D ROI-based approach. Compared to the 3D subject-level approach, this method works better for sMCI vs pMCI.

6.1.4. 2D slice-level

In general, the performance of the 2D-slice level approach was lower to that of the 3D ROI-based, 3D patch-level multi CNN and 3D subject-level (when trained with longitudinal data) approaches but higher than that of the 3D patch-level single CNN approach. For 2D slice-level, the use of longitudinal data for training did not improve the performance (0.79 ± 0.04 for baseline data; 0.79 ± 0.05 for longitudinal data). Finally, we studied the influence of data leakage using a slice-level data split strategy. As expected, the accuracy was 1.00 ± 0.00 .

6.1.5. Linear SVM

For task AD vs CN, the accuracies were 0.85 ± 0.02 when trained with baseline data and 0.85 ± 0.01 when trained with longitudinal data. For task sMCI vs pMCI, when training from scratch, the accuracies were 0.69 ± 0.02 when trained with baseline data and 0.68 ± 0.07 when trained with longitudinal data. When using transfer learning from the task AD vs CN to the task sMCI vs pMCI, the accuracies were 0.72 ± 0.04 (when trained with baseline data) and 0.69 ± 0.03 (when trained with longitudinal data). The performance of the SVM on AD vs CN is thus higher than that of most DL models and comparable to the best ones. Whereas for task sMCI vs pMCI, the accuracy of the SVM is lower than that of DL models.

6.2. Results on the test sets

Results on the three test sets (ADNI, OASIS and AIBL) are presented in Table 6. For each category of approach, we only applied the best models for both baseline and longitudinal data. The results will be computed and presented after the end of the peer-review process.

7. Discussion

The present studies contains three main contributions. First, we performed a systematic and critical literature review, which highlighted several important problems. Then, we proposed an open-source framework for the reproducible evaluation of AD classification using CNNs and T1w MRI. Finally, we applied the framework to rigorously compare different CNN approaches and to study the impact of key components on the performances. We hope that the present paper will provide a more objective assessment of the performance of CNN for AD classification and constitute a solid baseline for future research.

This paper first proposes a survey of existing CNN methods for AD classification. We hope to provide a useful overview of the different strategies. However, the survey highlighted several serious problems with the existing literature. First, we found that data leakage was potentially present in half of the 32 surveyed studies. This problem was evident in six of them and possible (due to inadequate description of the validation procedure) in ten others. This is a very serious issue, in particular considering that all these studies have undergone peer-review. This was likely to bias the performance upwards. In addition, in our experiments, we simulated one type of data leakage and found, as expected, that it led to a biased evaluation of the accuracy (1.00 instead of 0.79). Similar findings were observed in (Bäckström et al., 2018). Moreover, the survey highlighted that many studies did not motivate the choice of their architecture or training hyperparameters. Only two of them (Wang et al., 2019; S.-H. Wang et al., 2018) explored and gave results obtained with different architecture hyperparameters. However, it is possible that these performances were computed on the test set to help choosing their final model, hence they may be contaminated by data leakage. For other studies, it is also likely that they tried multiple number of choices leading to biased performances on the test set. We believe that these issues may potentially be caused by the lack of expertise in medical imaging or DL. For instance, splitting at the slice-level comes from a lack of knowledge of the nature of medical imaging data. We hope that the present paper will help to spread knowledge and good practices in the field.

Then, we proposed an open-source framework for reproducible experiments on AD classification using CNN. Some studies in our bibliography also provided their code on open source platforms (Hon and Khan, 2017; Hosseini-Asl et al., 2016; Korolev et al., 2017; Manhua Liu et al., 2018). Of note, two studies (Cheng and Liu, 2017; Manhua Liu et al., 2018) used the online code of (Hosseini-Asl et al., 2016) to compare to their framework and neither of them succeeded in reproducing the results of the original study (for the AD vs CN task they report both an accuracy of 0.82 while the original study reports an accuracy of 0.99). Our framework comprises unified tools for data management using the community standard BIDS (Gorgolewski et al., 2016), modular preprocessing pipelines, a set of CNN models which are representative of the literature and rigorous validation procedures. It builds upon our previously proposed framework but extends it to DL techniques (Samper-González et al., 2018; J. Wen et al., 2018). We hope to contribute in improving the reproducibility and objectivity in application of AD classification using DL methods. Our open-source framework facilitates the reproducible and objective evaluation of performances. It also allows to rigorously study the impact of the different components. Calls and emphasises have been made on reproducibility in both neuroimaging (Gorgolewski and Poldrack, 2016; Poldrack et al., 2017) and ML (Sonnenburg et al., 2007; Stodden et al., 2014; Vanschoren et al., 2014). We hope that our framework will be useful to future research in the field. Indeed, researchers can easily embed new CNN architectures or image preprocessing pipelines and study their added value.

We then demonstrated the use of our framework on three public datasets. Through this, we aim to provide a trustworthy baseline performance for the community. On the validation dataset, the diagnostic accuracy of CNNs ranged from 0.72 to 0.86 for task AD vs CN and from 0.74 to 0.80 for task sMCI vs pMCI, respectively. These baseline performances are in line with the state-of-the-art results (studies without data leakage in Table 1A), where classification accuracy typically ranged from 0.76 to 0.91 for the task AD vs CN and 0.62 to 0.83 for the task sMCI vs pMCI.

Different approaches, namely 3D subject-level, 3D ROI-based, 3D patch-level and 2D slice-level CNNs, were compared. Our study is the first one to systematically compare the performances of the four approaches. In the literature, three studies (Cheng et al., 2017; Li et al., 2018; Manhua Liu et al., 2018) using a

3D patch-level approach compared their results with a 3D subject-level approach. In all studies, the 3D patch-level multi-CNN gave better results than the 3D-subject CNN (3 or 4 percent points of difference between the two approaches). However, except for Liu et al (Manhua Liu et al., 2018) who reused the code provided by (Hosseini-Asl et al., 2016), the methods used for the comparison are poorly described and the studies would thus be difficult, if not impossible, to reproduce. In general, in our comparative study, the 3D ROI-based approach provided the best performances. The 3D subject-level CNN was competitive with 3D ROI-based for AD vs CN classification but not for sMCI vs pMCI. The superior performance of the ROI-based approach may appear surprising since it uses only a specific portion of the brain (the hippocampus) while 3D subject-level approach uses all information available. Indeed, even though the hippocampus is affected early and severely by AD (Braak and Braak, 1998), alterations in AD are not confined to the hippocampus and extend to other regions in the temporal, parietal and frontal lobes. A previous comparative study, using different types of ML techniques but not CNN, has shown that whole-brain approaches are more effective than methods using only the hippocampus (Cuingnet et al., 2011). In the case of DL, it is possible that the ROI-based CNNs work better because they are less complex (fewer learnt parameters) than the 3D subject-level CNNs, thus leading to less overfitting. It may thus be that whole brain approaches would result in higher performance when trained on larger samples. Two papers in the literature using hippocampal ROI reported high accuracies for task AD vs CN (0.84 and 0.90), comparable to ours, even though their definition of the ROI was different (Aderghal et al., 2018, 2017c). As for the 3D subjects (Bäckström et al., 2018; Cheng and Liu, 2017; Korolev et al., 2017; Li et al., 2017; Senanayake et al., 2018; Shmulev et al., 2018), results of the literature varied across papers, from 0.76 to 0.90. Although we cannot prove it directly, we believe that this variability stems from the high risk of overfitting. Moreover, 3D patch-level and 2D slice-level approaches led to lower accuracies compared to 3D ROI-based or 3D subject-level CNNs. One can hypothesize that this is because the spatial information is not adequately modeled by these approaches (no 3D consistency between slices, no consistency at the border of patches). Other studies with 3D patch-level approaches in the literature (Cheng et al., 2017; Lian et al., 2018; Li et al., 2018; Mingxia Liu et al., 2018a, 2018c) reported higher accuracies (from 0.87 to 0.91) than ours (0.81). We hypothesize that it may come from the increased complexity of their approach, including patch selection and fusion. Only one paper (without data leakage) has explored 2D slice-level using ImageNet pre-trained ResNet (Valliani and Soni, 2017). Their accuracy is very similar to ours (0.81 for task AD vs CN). Here, we provided a direct comparison with other approaches and demonstrated that a 2D slice-level approach leads to lower performances compared to 3D ROI-based or 3D subject-level CNNs.

For the 3D patch-level, we showed that the multi-CNN approach (0.81) was superior to the single-CNN approach (0.72). This is probably because fitting all patches/slices into one single CNN could lead to losing the voxel correspondence across patches/slices. However, the multi-CNN approach (0.81) obtained lower accuracies compared to the 3D subject-level approach (0.85).

After the peer-review process, when the results on the three test datasets have been obtained, we will include a paragraph discussing the results on the test dataset and the implications for the generalizability of the models. We will discuss both generalizability to unseen data of the same study (ADNI) and to other studies with similar (AIBL) or different (OASIS) inclusion criteria and imaging parameters.

We studied the influence of several key choices on the performance. First, we studied the influence of AE pre-training and showed that it did not improve the average accuracy over training from scratch. However, AE pre-training resulted in a lower variance over the 5-folds of the CV. Three previous papers studied the impact of AE pre-training (Hosseini-Asl et al., 2016; Vu et al., 2018, 2017) and found that it improved the results. However, they are all at least suspected of data leakage. We thus conclude that, to date, it is not proven that AE pre-training leads to increased average accuracy. A difficulty in AD classification using DL is the limited data sample for training. We demonstrated that training with longitudinal data gave superior (3D subject-level) or comparable (other approaches) performances compared to baseline data. This discrepancy across approaches may come from the fact that 3D subject-level CNNs were more complex (more learnt parameters) than other approaches, and thus that more training data has more impact on this approach. The absence of improvement for the majority of cases may be due to several factors. First, training with longitudinal data implies training with data from more advanced disease stages, since patients are seen at a later point in the disease course. This may have an adverse effect on the performance of the model when tested

on baseline data, at which the patients are less advanced. Also, since the additional data come from the same patient, this does not provide a better coverage of inter-individual variability. We studied the impact of image preprocessing. First, as expected, we found that CNNs cannot be successfully trained without intensity rescaling. We then studied the influence of two different procedures (“Minimal” and “Extensive”). Of note, “Extensive” procedure requires redundantly a non-linear registration, instead of a linear one, and skull stripping compared to “Minimal” procedure. They led to comparable results. In principle, this is not surprising as DL methods do not require extensive preprocessing. In the literature, varied types of preprocessing have been used. Some studies used non-linear registration (Bäckström et al., 2018; Basaia et al., 2019; Lian et al., 2018; Lin et al., 2018; Mingxia Liu et al., 2018a, 2018c; Wang et al., 2019; S.-H. Wang et al., 2018) while others used only linear (Aderghal et al., 2018, 2017a, 2017b; Hosseini Asl et al., 2018; Li et al., 2018; Manhua Liu et al., 2018; Shmulev et al., 2018) or no registration (Cheng and Liu, 2017). None of them compared these different preprocessings with the exception of (Bäckström et al., 2018) which compared preprocessed data using FreeSurfer to no preprocessing. They found that training the network with the raw data obtained inferior classification performance (38% drop for accuracy) compared to the preprocessed data using FreeSurfer (Bäckström et al., 2018). However, FreeSurfer comprises a complex pipeline with many preprocessing steps so it is unclear, from their results, which part drives the superior performance.

One interesting question is whether DL could perform better than conventional ML methods for AD classification. Here, we chose to compare CNN to a linear SVM. SVM has been used in many AD classification studies and obtained competitive performances (Falahati et al., 2014; Haller et al., 2011; Rathore et al., 2017). In the current study, compared to SVM, CNN gave comparable performances for task AD vs CN and superior performances for task sMCI vs pMCI. Note that we used a standard linear SVM with standard voxel-based features. For task AD vs CN, we do not claim that possibly more sophisticated DL architectures would not outperform the SVM. However, this is not the case with the architectures that we tested which are representative of the existing literature on AD classification. Besides, it is possible that CNN will outperform SVM when larger public dataset are available in the future. On the other hand, the CNN outperformed the SVM for the most difficult (and more interesting) sMCI vs pMCI classification task (0.80 vs 0.72). This is an interesting result which demonstrates the potential of DL for challenging diagnostic tasks.

Unbiased evaluation of the performances is an essential task in ML. This is particularly critical for deep learning because of the extreme flexibility of the models and the numerous possible choices that can be made regarding architecture and hyperparameter choices. In particular, it is crucial that such choices are not made using the test set. We chose a very strict validation strategy in that respect: the test sets were left untouched until the end of the peer-review process. This guarantees that only the final models, after all possible adjustments, are carried to the test set. Moreover, it is important to assess generalization not only to unseen subjects but also to other studies in which image acquisitions or patient inclusion criteria can vary. In the present paper, we used three test sets from ADNI, AIBL and OASIS to assess generalization to these different conditions.

Our study has the following limitations. First, a very large number of different choices can be made regarding the model architecture and training hyperparameters. Even though we did our best efforts to make meaningful choices and for testing a relatively large number of possibilities, we cannot exclude that other choices could have led to better results. [Note to reviewers: suggestions for other choices are welcome, as long as they are within a reasonable number]. To overcome this limitation, our framework is freely available to the community. We will thus hope that other researchers will use it to propose and validate potentially better performing models. In particular, with our proposed framework, researchers can easily try their own models without touching the concealed test dataset. Secondly, the CV procedures were performed only once. Of course, the training is not deterministic and one would ideally want to repeat the CV to get a more robust estimate of the performance. However, we did not perform this due to limited computational resources. Finally, overfitting always exist in our experiments, albeit different techniques have been tried (e.g. transfer learning, dropout or weight decay). This phenomenon occurs mainly due to our small data sample in AD classification. It is likely that training with much larger datasets would result in higher performance models. However, in the field of AD, such very large datasets are not yet publicly available.

Acknowledgements

We thank Mr. Maxime Kermarquer for the IT support during this study. We also thank the following colleagues for useful discussions and suggestions: Alexandre Bône and Johann Faouzi. The research leading to these results has received funding from the program “Investissements d’avenir” ANR-10-IAIHU-06 (Agence Nationale de la Recherche-10-IA Agence Institut Hospitalo-Universitaire-6), from the European Union H2020 program (project EuroPOND, grant number 666992), and from the joint NSF/NIH/ANR program “Collaborative Research in Computational Neuroscience” (project HIPLAY7, grant number ANR-16-NEUC-0001-01). J.W. receives financial support from China Scholarship Council (CSC). O.C. is supported by a “Contrat d’Interface Local” from Assistance Publique-Hôpitaux de Paris (AP-HP).

Data collection and sharing for this project was funded by the Alzheimer's Disease Neuroimaging Initiative (ADNI) (National Institutes of Health Grant U01 AG024904) and DOD ADNI (Department of Defense award number W81XWH-12-2-0012). ADNI is funded by the National Institute on Aging, the National Institute of Biomedical Imaging and Bioengineering, and through generous contributions from the following: AbbVie, Alzheimer’s Association; Alzheimer’s Drug Discovery Foundation; Araclon Biotech; BioClinica, Inc.; Biogen; Bristol-Myers Squibb Company; CereSpir, Inc.; Cogstate; Eisai Inc.; Elan Pharmaceuticals, Inc.; Eli Lilly and Company; EuroImmun; F. Hoffmann-La Roche Ltd and its affiliated company Genentech, Inc.; Fujirebio; GE Healthcare; IXICO Ltd.; Janssen Alzheimer Immunotherapy Research & Development, LLC.; Johnson & Johnson Pharmaceutical Research & Development LLC.; Lumosity; Lundbeck; Merck & Co., Inc.; Meso Scale Diagnostics, LLC.; NeuroRx Research; Neurotrack Technologies; Novartis Pharmaceuticals Corporation; Pfizer Inc.; Piramal Imaging; Servier; Takeda Pharmaceutical Company; and Transition Therapeutics. The Canadian Institutes of Health Research is providing funds to support ADNI clinical sites in Canada. Private sector contributions are facilitated by the Foundation for the National Institutes of Health (www.fnih.org). The grantee organization is the Northern California Institute for Research and Education, and the study is coordinated by the Alzheimer’s Therapeutic Research Institute at the University of Southern California. ADNI data are disseminated by the Laboratory for Neuro Imaging at the University of Southern California. The OASIS Cross-Sectional project (Principal Investigators: D. Marcus, R. Buckner, J. Csernansky J. Morris) was supported by the following grants: P50 AG05681, P01 AG03991, P01 AG026276, R01 AG021910, P20 MH071616, and U24 RR021382.

References

- Aderghal, K., Benois-Pineau, J., Afdel, K., Gwenaëlle, C., 2017a. FuseMe: Classification of sMRI images by fusion of Deep CNNs in 2D+ ϵ projections, in: Proceedings of the 15th International Workshop on Content-Based Multimedia Indexing. ACM, p. 34. <https://doi.org/10.1145/3095713.3095749>
- Aderghal, K., Boissenin, M., Benois-Pineau, J., Catheline, G., Afdel, K., 2017b. Classification of sMRI for AD Diagnosis with Convolutional Neuronal Networks: A Pilot 2-D+ ϵ Study on ADNI, in: Amsaleg, L., Guðmundsson, G.P., Gurrin, C., Jónsson, B.P., Satoh, S. (Eds.), MultiMedia Modeling, Lecture Notes in Computer Science. Springer International Publishing, Cham, pp. 690–701. https://doi.org/10.1007/978-3-319-51811-4_56
- Aderghal, K., Boissenin, M., Benois-Pineau, J., Catheline, G., Afdel, K., 2017c. Classification of sMRI for AD Diagnosis with Convolutional Neuronal Networks: A Pilot 2-D+ ϵ Study on ADNI, in: International Conference on Multimedia Modeling. Springer, pp. 690–701.
- Aderghal, K., Khvostikov, A., Krylov, A., Benois-Pineau, J., Afdel, K., Catheline, G., 2018. Classification of Alzheimer Disease on Imaging Modalities with Deep CNNs Using Cross-Modal Transfer Learning, in: 2018 IEEE 31st International Symposium on Computer-Based Medical Systems (CBMS). pp. 345–350. <https://doi.org/10.1109/CBMS.2018.00067>
- Aisen, P.S., Petersen, R.C., Donohue, M.C., Gamst, A., Raman, R., Thomas, R.G., Walter, S., Trojanowski, J.Q., Shaw, L.M., Beckett, L.A., Jack, C.R., Jr, Jagust, W., Toga, A.W., Saykin, A.J., Morris, J.C., Green, R.C., Weiner, M.W., Alzheimer's Disease Neuroimaging Initiative, 2010. Clinical Core of the Alzheimer's Disease Neuroimaging Initiative: progress and plans. *Alzheimers. Dement.* 6, 239–246. <https://doi.org/10.1016/j.jalz.2010.03.006>
- Amoroso, N., Diacono, D., Fanizzi, A., La Rocca, M., Monaco, A., Lombardi, A., Guaragnella, C., Bellotti, R., Tangaro, S., Alzheimer's Disease Neuroimaging Initiative, 2018. Deep learning reveals Alzheimer's disease onset in MCI subjects: Results from an international challenge. *J. Neurosci. Methods* 302, 3–9. <https://doi.org/10.1016/j.jneumeth.2017.12.011>
- Andersson, J.L.R., Jenkinson, M., Smith, S., 2010. Non-linear registration aka Spatial normalisation. FMRIB Technial Report TR07JA2.
- Ashburner, J., 2007. A fast diffeomorphic image registration algorithm. *Neuroimage* 38, 95–113. <https://doi.org/10.1016/j.neuroimage.2007.07.007>
- Ashburner, J., Friston, K.J., 2005. Unified segmentation. *Neuroimage* 26, 839–851. <https://doi.org/10.1016/j.neuroimage.2005.02.018>
- Ashburner, J., Friston, K.J., 2000. Voxel-Based Morphometry—The Methods. *Neuroimage* 11, 805–821. <https://doi.org/10.1006/nimg.2000.0582>
- Avants, B.B., Epstein, C.L., Grossman, M., Gee, J.C., 2008. Symmetric diffeomorphic image registration with cross-correlation: evaluating automated labeling of elderly and neurodegenerative brain. *Med. Image Anal.* 12, 26–41. <https://doi.org/10.1016/j.media.2007.06.004>
- Avants, B.B., Tustison, N.J., Stauffer, M., Song, G., Wu, B., Gee, J.C., 2014. The Insight ToolKit image registration framework. *Front. Neuroinform.* 8, 44. <https://doi.org/10.3389/fninf.2014.00044>
- Bäckström, K., Nazari, M., Gu, I.Y., Jakola, A.S., 2018. An efficient 3D deep convolutional network for Alzheimer's disease diagnosis using MR images, in: 2018 IEEE 15th International Symposium on Biomedical Imaging (ISBI 2018). pp. 149–153. <https://doi.org/10.1109/ISBI.2018.8363543>
- Bankman, I., 2008. Handbook of Medical Image Processing and Analysis. Elsevier.
- Basaia, S., Agosta, F., Wagner, L., Canu, E., Magnani, G., Santangelo, R., Filippi, M., Alzheimer's Disease Neuroimaging Initiative, 2019. Automated classification of Alzheimer's disease and mild cognitive impairment using a single MRI and deep neural networks. *Neuroimage Clin* 21, 101645. <https://doi.org/10.1016/j.nicl.2018.101645>
- Baskar, D., Jayanthi, V.S., Jayanthi, A.N., 2018. An efficient classification approach for detection of Alzheimer's disease from biomedical imaging modalities. *Multimed. Tools Appl.* 1–33. <https://doi.org/10.1007/s11042-018-6287-8>
- Bernal, J., Kushibar, K., Asfaw, D.S., Valverde, S., Oliver, A., Martí, R., Lladó, X., 2018. Deep convolutional neural networks for brain image analysis on magnetic resonance imaging: a review. *Artif. Intell. Med.* <https://doi.org/10.1016/j.artmed.2018.08.008>

- Bhagwat, N., Viviano, J.D., Voineskos, A.N., Chakravarty, M.M., Alzheimer's Disease Neuroimaging Initiative, 2018. Modeling and prediction of clinical symptom trajectories in Alzheimer's disease using longitudinal data. *PLoS Comput. Biol.* 14, e1006376. <https://doi.org/10.1371/journal.pcbi.1006376>
- Bourlard, H., Kamp, Y., 1988. Auto-association by multilayer perceptrons and singular value decomposition. *Biol. Cybern.* 59, 291–294. <https://doi.org/10.1007/bf00332918>
- Braak, H., Braak, E., 1998. Evolution of neuronal changes in the course of Alzheimer's disease, in: Jellinger, K., Fazekas, F., Windisch, M. (Eds.), *Ageing and Dementia*, Journal of Neural Transmission. Supplementa. Springer Vienna, Vienna, pp. 127–140. https://doi.org/10.1007/978-3-7091-6467-9_11
- Brookmeyer, R., Johnson, E., Ziegler-Graham, K., Arrighi, H.M., 2007. Forecasting the global burden of Alzheimer's disease. *Alzheimers. Dement.* 3, 186–191. <https://doi.org/10.1016/j.jalz.2007.04.381>
- Cárdenas-Peña, D., Collazos-Huertas, D., Castellanos-Dominguez, G., 2017. Enhanced Data Representation by Kernel Metric Learning for Dementia Diagnosis. *Front. Neurosci.* 11, 413. <https://doi.org/10.3389/fnins.2017.00413>
- Cárdenas-Peña, D., Collazos-Huertas, D., Castellanos-Dominguez, G., 2016. Centered Kernel Alignment Enhancing Neural Network Pretraining for MRI-Based Dementia Diagnosis. *Comput. Math. Methods Med.* 2016, 9523849. <https://doi.org/10.1155/2016/9523849>
- Chaddad, A., Desrosiers, C., Niazi, T., 2018. Deep Radiomic Analysis of MRI Related to Alzheimer's Disease. *IEEE Access* 6, 58213–58221. <https://doi.org/10.1109/ACCESS.2018.2871977>
- Cheng, D., Liu, M., 2017. CNNs based multi-modality classification for AD diagnosis, in: 2017 10th International Congress on Image and Signal Processing, BioMedical Engineering and Informatics (CISP-BMEI). pp. 1–5. <https://doi.org/10.1109/CISP-BMEI.2017.8302281>
- Cheng, D., Liu, M., Fu, J., Wang, Y., 2017. Classification of MR brain images by combination of multi-CNNs for AD diagnosis, in: Ninth International Conference on Digital Image Processing (ICDIP 2017). Presented at the Ninth International Conference on Digital Image Processing (ICDIP 2017), International Society for Optics and Photonics, p. 1042042. <https://doi.org/10.1117/12.2281808>
- Ciresan, D.C., Meier, U., Masci, J., Maria Gambardella, L., Schmidhuber, J., 2011. Flexible, high performance convolutional neural networks for image classification, in: *IJCAI Proceedings-International Joint Conference on Artificial Intelligence*. Barcelona, Spain, p. 1237.
- Çitak-ER, F., Goularas, D., Ormeci, B., 2017. A novel Convolutional Neural Network Model Based on Voxel-based Morphometry of Imaging Data in Predicting the Prognosis of Patients with Mild Cognitive Impairment. *J. Neurol. Sci. Turk.* 34.
- Cuingnet, R., Gerardin, E., Tessieras, J., Auzias, G., Lehéricy, S., Habert, M.-O., Chupin, M., Benali, H., Colliot, O., Alzheimer's Disease Neuroimaging Initiative, 2011. Automatic classification of patients with Alzheimer's disease from structural MRI: a comparison of ten methods using the ADNI database. *Neuroimage* 56, 766–781. <https://doi.org/10.1016/j.neuroimage.2010.06.013>
- Cui, R., Liu, M., Li, G., 2018. Longitudinal analysis for Alzheimer's disease diagnosis using RNN, in: 2018 IEEE 15th International Symposium on Biomedical Imaging (ISBI 2018). pp. 1398–1401. <https://doi.org/10.1109/ISBI.2018.8363833>
- de Boer, P.-T., Kroese, D.P., Mannor, S., Rubinstein, R.Y., 2005. A Tutorial on the Cross-Entropy Method. *Ann. Oper. Res.* 134, 19–67. <https://doi.org/10.1007/s10479-005-5724-z>
- Deng, J., Dong, W., Socher, R., Li, L.-J., Li, K., Fei-Fei, L., 2009. ImageNet: A large-scale hierarchical image database. 2009 IEEE Conference on Computer Vision and Pattern Recognition. <https://doi.org/10.1109/cvprw.2009.5206848>
- Dickerson, B.C., Goncharova, I., Sullivan, M.P., Forchetti, C., Wilson, R.S., Bennett, D.A., Beckett, L.A., Others, 2001. MRI-derived entorhinal and hippocampal atrophy in incipient and very mild Alzheimer's disease ☆. *Neurobiol. Aging* 22, 747–754.
- Dolph, C.V., Alam, M., Shboul, Z., Samad, M.D., Iftekharuddin, K.M., 2017. Deep learning of texture and structural features for multiclass Alzheimer's disease classification, in: 2017 International Joint Conference on Neural Networks (IJCNN). pp. 2259–2266. <https://doi.org/10.1109/IJCNN.2017.7966129>
- Dumoulin, V., Visin, F., 2016. A guide to convolution arithmetic for deep learning. *arXiv [stat.ML]*.
- Duraisamy, B., Shanmugam, J.V., Annamalai, J., 2019. Alzheimer disease detection from structural MR images using FCM based weighted probabilistic neural network. *Brain Imaging Behav.* 13, 87–110. <https://doi.org/10.1007/s11682-018-9831-2>
- Ellis, K.A., Bush, A.I., Darby, D., De Fazio, D., Foster, J., Hudson, P., Lautenschlager, N.T., Lenzo, N.,

- Martins, R.N., Maruff, P., Others, 2009. The Australian Imaging, Biomarkers and Lifestyle (AIBL) study of aging: methodology and baseline characteristics of 1112 individuals recruited for a longitudinal study of Alzheimer's disease. *Int. Psychogeriatr.* 21, 672–687.
- Ellis, K.A., Rowe, C.C., Villemagne, V.L., Martins, R.N., Masters, C.L., Salvado, O., Szoek, C., Ames, D., 2010. Addressing population aging and Alzheimer's disease through the Australian Imaging Biomarkers and Lifestyle study: Collaboration with the Alzheimer's Disease Neuroimaging Initiative. *Alzheimer's & Dementia.* <https://doi.org/10.1016/j.jalz.2010.03.009>
- Erhan, D., Bengio, Y., Courville, A., Manzagol, P.-A., Vincent, P., Bengio, S., 2010. Why Does Unsupervised Pre-training Help Deep Learning? *J. Mach. Learn. Res.* 11, 625–660.
- Esmailzadeh, S., Belivanis, D.I., Pohl, K.M., Adeli, E., 2018. End-To-End Alzheimer's Disease Diagnosis and Biomarker Identification: 9th International Workshop, MLMI 2018, Held in Conjunction with MICCAI 2018, Granada, Spain, September 16, 2018, Proceedings, in: Shi, Y., Suk, H.-I., Liu, M. (Eds.), *Machine Learning in Medical Imaging, Lecture Notes in Computer Science.* Springer International Publishing, Cham, pp. 337–345. https://doi.org/10.1007/978-3-030-00919-9_39
- Ewers, M., Sperling, R.A., Klunk, W.E., Weiner, M.W., Hampel, H., 2011. Neuroimaging markers for the prediction and early diagnosis of Alzheimer's disease dementia. *Trends Neurosci.* 34, 430–442. <https://doi.org/10.1016/j.tins.2011.05.005>
- Falahati, F., Westman, E., Simmons, A., 2014. Multivariate data analysis and machine learning in Alzheimer's disease with a focus on structural magnetic resonance imaging. *J. Alzheimers. Dis.* 41, 685–708. <https://doi.org/10.3233/JAD-131928>
- Farooq, A., Anwar, S., Awais, M., Rehman, S., 2017. A deep CNN based multi-class classification of Alzheimer's disease using MRI, in: 2017 IEEE International Conference on Imaging Systems and Techniques (IST). pp. 1–6. <https://doi.org/10.1109/IST.2017.8261460>
- Fonov, V., Dadar, M., The PREVENT-AD Research Group, Louis Collins, D., 2018. Deep learning of quality control for stereotaxic registration of human brain MRI. *bioRxiv.* <https://doi.org/10.1101/303487>
- Fonov, V., Evans, A.C., Botteron, K., Almlí, C.R., McKinstry, R.C., Collins, D.L., Brain Development Cooperative Group, 2011. Unbiased average age-appropriate atlases for pediatric studies. *Neuroimage* 54, 313–327. <https://doi.org/10.1016/j.neuroimage.2010.07.033>
- Fonov, V.S., Evans, A.C., McKinstry, R.C., Almlí, C.R., Collins, D.L., 2009. Unbiased nonlinear average age-appropriate brain templates from birth to adulthood. *Neuroimage Supplement 1*, S102. [https://doi.org/10.1016/S1053-8119\(09\)70884-5](https://doi.org/10.1016/S1053-8119(09)70884-5)
- Friston, K.J., Holmes, A.P., Poline, J.B., Grasby, P.J., Williams, S.C., Frackowiak, R.S., Turner, R., 1995. Analysis of fMRI time-series revisited. *Neuroimage* 2, 45–53. <https://doi.org/10.1006/nimg.1995.1007>
- Glorot, X., Bordes, A., Bengio, Y., 2011. Deep sparse rectifier neural networks, in: Proceedings of the Fourteenth International Conference on Artificial Intelligence and Statistics. pp. 315–323.
- Goodfellow, I., 2016. NIPS 2016 Tutorial: Generative Adversarial Networks. *arXiv [cs.LG].*
- Goodfellow, I., Bengio, Y., Courville, A., Bengio, Y., 2016. *Deep learning.* MIT press Cambridge.
- Gorgolewski, K., Burns, C.D., Madison, C., Clark, D., Halchenko, Y.O., Waskom, M.L., Ghosh, S.S., 2011. Nipype: a flexible, lightweight and extensible neuroimaging data processing framework in python. *Front. Neuroinform.* 5, 13. <https://doi.org/10.3389/fninf.2011.00013>
- Gorgolewski, K.J., Auer, T., Calhoun, V.D., Craddock, R.C., Das, S., Duff, E.P., Flandin, G., Ghosh, S.S., Glatard, T., Halchenko, Y.O., Handwerker, D.A., Hanke, M., Keator, D., Li, X., Michael, Z., Maumet, C., Nichols, B.N., Nichols, T.E., Pellman, J., Poline, J.-B., Rokem, A., Schaefer, G., Sochat, V., Triplett, W., Turner, J.A., Varoquaux, G., Poldrack, R.A., 2016. The brain imaging data structure, a format for organizing and describing outputs of neuroimaging experiments. *Sci Data* 3, 160044. <https://doi.org/10.1038/sdata.2016.44>
- Gorgolewski, K.J., Poldrack, R.A., 2016. A Practical Guide for Improving Transparency and Reproducibility in Neuroimaging Research. *PLoS Biol.* 14, e1002506. <https://doi.org/10.1371/journal.pbio.1002506>
- Gorji, H.T., Haddadnia, J., 2015. A novel method for early diagnosis of Alzheimer's disease based on pseudo Zernike moment from structural MRI. *Neuroscience* 305, 361–371. <https://doi.org/10.1016/j.neuroscience.2015.08.013>
- Greve, D.N., Fischl, B., 2009. Accurate and robust brain image alignment using boundary-based registration. *Neuroimage* 48, 63–72. <https://doi.org/10.1016/j.neuroimage.2009.06.060>
- Gunawardena, K.A.N.N.P., Rajapakse, R.N., Kodikara, N.D., 2017. Applying convolutional neural networks

- for pre-detection of alzheimer's disease from structural MRI data, in: 2017 24th International Conference on Mechatronics and Machine Vision in Practice (M2VIP). pp. 1–7.
<https://doi.org/10.1109/M2VIP.2017.8211486>
- Gutiérrez-Becker, B., Wachinger, C., 2018. Deep Multi-structural Shape Analysis: Application to Neuroanatomy: 21st International Conference, Granada, Spain, September 16-20, 2018, Proceedings, Part III, in: Frangi, A.F., Schnabel, J.A., Davatzikos, C., Alberola-López, C., Fichtinger, G. (Eds.), Medical Image Computing and Computer Assisted Intervention – MICCAI 2018, Lecture Notes in Computer Science. Springer International Publishing, Cham, pp. 523–531.
https://doi.org/10.1007/978-3-030-00931-1_60
- Haller, S., Lovblad, K.O., Giannakopoulos, P., 2011. Principles of classification analyses in mild cognitive impairment (MCI) and Alzheimer disease. *J. Alzheimers. Dis.* 26 Suppl 3, 389–394.
<https://doi.org/10.3233/JAD-2011-0014>
- He, K., Zhang, X., Ren, S., Sun, J., 2016. Deep residual learning for image recognition, in: Proceedings of the IEEE Conference on Computer Vision and Pattern Recognition. pp. 770–778.
- Hinton, G.E., Zemel, R.S., 1994. Autoencoders, Minimum Description Length and Helmholtz Free Energy, in: Cowan, J.D., Tesauro, G., Alspector, J. (Eds.), Advances in Neural Information Processing Systems 6. Morgan-Kaufmann, pp. 3–10.
- Hon, M., Khan, N.M., 2017. Towards Alzheimer's disease classification through transfer learning, in: 2017 IEEE International Conference on Bioinformatics and Biomedicine (BIBM). pp. 1166–1169.
<https://doi.org/10.1109/BIBM.2017.8217822>
- Hosseini Asl, E., Ghazal, M., Mahmoud, A., Aslantas, A., Shalaby, A., Casanova, M., Barnes, G., Gimel'farb, G., Keynton, R., El Baz, A., 2018. Alzheimer's disease diagnostics by a 3D deeply supervised adaptable convolutional network. *Front. Biosci.* 23, 584–596. <https://doi.org/10.2741/4606>
- Hosseini-Asl, E., Keynton, R., El-Baz, A., 2016. Alzheimer's disease diagnostics by adaptation of 3D convolutional network, in: 2016 IEEE International Conference on Image Processing (ICIP). pp. 126–130. <https://doi.org/10.1109/ICIP.2016.7532332>
- Huang, G., Liu, Z., Van Der Maaten, L., Weinberger, K.Q., 2017. Densely connected convolutional networks, in: Proceedings of the IEEE Conference on Computer Vision and Pattern Recognition. pp. 4700–4708.
- Ioffe, S., Szegedy, C., 2015. Batch Normalization: Accelerating Deep Network Training by Reducing Internal Covariate Shift. *arXiv [cs.LG]*.
- Islam, J., Zhang, Y., 2018. Brain MRI analysis for Alzheimer's disease diagnosis using an ensemble system of deep convolutional neural networks. *Brain Inform* 5, 2. <https://doi.org/10.1186/s40708-018-0080-3>
- Islam, J., Zhang, Y., 2017. A Novel Deep Learning Based Multi-class Classification Method for Alzheimer's Disease Detection Using Brain MRI Data, in: Zeng, Y., He, Y., Kotaleski, J.H., Martone, M., Xu, B., Peng, H., Luo, Q. (Eds.), Brain Informatics, Lecture Notes in Computer Science. Springer International Publishing, Cham, pp. 213–222. https://doi.org/10.1007/978-3-319-70772-3_20
- Janocha, K., Czarnecki, W.M., 2017. On Loss Functions for Deep Neural Networks in Classification. *arXiv [cs.LG]*.
- Jenkinson, M., Bannister, P., Brady, M., Smith, S., 2002. Improved optimization for the robust and accurate linear registration and motion correction of brain images. *Neuroimage* 17, 825–841.
- Jenkinson, M., Smith, S., 2001. A global optimisation method for robust affine registration of brain images. *Med. Image Anal.* 5, 143–156.
- Jha, D., Kim, J.-I., Kwon, G.-R., 2017. Diagnosis of Alzheimer's Disease Using Dual-Tree Complex Wavelet Transform, PCA, and Feed-Forward Neural Network. *J. Healthc. Eng.* 2017, 9060124.
<https://doi.org/10.1155/2017/9060124>
- Juszczak, P., Tax, D., Duin, R.P.W., 2002. Feature scaling in support vector data description, in: Proc. ASCI. Citeseer, pp. 95–102.
- Kalavathi, P., Prasath, V.B.S., 2016. Methods on Skull Stripping of MRI Head Scan Images-a Review. *J. Digit. Imaging* 29, 365–379. <https://doi.org/10.1007/s10278-015-9847-8>
- Korolev, S., Safiullin, A., Belyaev, M., Dodonova, Y., 2017. Residual and plain convolutional neural networks for 3D brain MRI classification, in: 2017 IEEE 14th International Symposium on Biomedical Imaging (ISBI 2017). pp. 835–838. <https://doi.org/10.1109/ISBI.2017.7950647>
- Kriegeskorte, N., Simmons, W.K., Bellgowan, P.S.F., Baker, C.I., 2009. Circular analysis in systems neuroscience: the dangers of double dipping. *Nat. Neurosci.* 12, 535–540.

<https://doi.org/10.1038/nn.2303>

- Krizhevsky, A., Sutskever, I., Hinton, G.E., 2012. ImageNet Classification with Deep Convolutional Neural Networks, in: Pereira, F., Burges, C.J.C., Bottou, L., Weinberger, K.Q. (Eds.), *Advances in Neural Information Processing Systems 25*. Curran Associates, Inc., pp. 1097–1105.
- Krogh, A., Hertz, J.A., 1992. A Simple Weight Decay Can Improve Generalization, in: Moody, J.E., Hanson, S.J., Lippmann, R.P. (Eds.), *Advances in Neural Information Processing Systems 4*. Morgan-Kaufmann, pp. 950–957.
- LeCun, Y., Bengio, Y., Hinton, G., 2015. Deep learning. *Nature* 521, 436–444.
<https://doi.org/10.1038/nature14539>
- Lecun, Y., Bottou, L., Bengio, Y., Haffner, P., 1998. Gradient-based learning applied to document recognition. *Proc. IEEE* 86, 2278–2324. <https://doi.org/10.1109/5.726791>
- Ledig, C., Heckemann, R.A., Hammers, A., Lopez, J.C., Newcombe, V.F.J., Makropoulos, A., Lötjönen, J., Menon, D.K., Rueckert, D., 2015. Robust whole-brain segmentation: application to traumatic brain injury. *Med. Image Anal.* 21, 40–58. <https://doi.org/10.1016/j.media.2014.12.003>
- Lian, C., Liu, M., Zhang, J., Shen, D., 2018. Hierarchical Fully Convolutional Network for Joint Atrophy Localization and Alzheimer’s Disease Diagnosis using Structural MRI. *IEEE Trans. Pattern Anal. Mach. Intell.* <https://doi.org/10.1109/TPAMI.2018.2889096>
- Li, F., Cheng, D., Liu, M., 2017. Alzheimer’s disease classification based on combination of multi-model convolutional networks, in: 2017 IEEE International Conference on Imaging Systems and Techniques (IST). pp. 1–5. <https://doi.org/10.1109/IST.2017.8261566>
- Li, F., Liu, M., Alzheimer’s Disease Neuroimaging Initiative, 2018. Alzheimer’s disease diagnosis based on multiple cluster dense convolutional networks. *Comput. Med. Imaging Graph.* 70, 101–110.
<https://doi.org/10.1016/j.compmedimag.2018.09.009>
- Li, F., Tran, L., Thung, K.-H., Ji, S., Shen, D., Li, J., 2015. A Robust Deep Model for Improved Classification of AD/MCI Patients. *IEEE J Biomed Health Inform* 19, 1610–1616.
<https://doi.org/10.1109/JBHI.2015.2429556>
- Lin, W., Tong, T., Gao, Q., Guo, D., Du, X., Yang, Y., Guo, G., Xiao, M., Du, M., Qu, X., Alzheimer’s Disease Neuroimaging Initiative, 2018. Convolutional Neural Networks-Based MRI Image Analysis for the Alzheimer’s Disease Prediction From Mild Cognitive Impairment. *Front. Neurosci.* 12, 777.
<https://doi.org/10.3389/fnins.2018.00777>
- Liu, J., Pan, Y., Li, M., Chen, Z., Tang, L., Lu, C., Wang, J., 2018. Applications of deep learning to MRI images: A survey. *Big Data Mining and Analytics* 1, 1–18.
<https://doi.org/10.26599/BDMA.2018.9020001>
- Liu, J., Shang, S., Zheng, K., Wen, J.-R., 2016. Multi-view ensemble learning for dementia diagnosis from neuroimaging: An artificial neural network approach. *Neurocomputing* 195, 112–116.
<https://doi.org/10.1016/j.neucom.2015.09.119>
- Liu, M., Cheng, D., Wang, K., Wang, Y., Alzheimer’s Disease Neuroimaging Initiative, 2018. Multi-Modality Cascaded Convolutional Neural Networks for Alzheimer’s Disease Diagnosis. *Neuroinformatics* 16, 295–308. <https://doi.org/10.1007/s12021-018-9370-4>
- Liu, M., Zhang, J., Adeli, E., Shen, D., 2018a. Landmark-based deep multi-instance learning for brain disease diagnosis. *Med. Image Anal.* 43, 157–168. <https://doi.org/10.1016/j.media.2017.10.005>
- Liu, M., Zhang, J., Adeli, E., Shen, D., 2018b. Joint Classification and Regression via Deep Multi-Task Multi-Channel Learning for Alzheimer’s Disease Diagnosis. *IEEE Trans. Biomed. Eng.*
<https://doi.org/10.1109/TBME.2018.2869989>
- Liu, M., Zhang, J., Nie, D., Yap, P.-T., Shen, D., 2018c. Anatomical Landmark Based Deep Feature Representation for MR Images in Brain Disease Diagnosis. *IEEE J Biomed Health Inform* 22, 1476–1485. <https://doi.org/10.1109/JBHI.2018.2791863>
- Liu, S., Liu, S., Cai, W., Che, H., Pujol, S., Kikinis, R., Feng, D., Fulham, M.J., ADNI, 2015. Multimodal neuroimaging feature learning for multiclass diagnosis of Alzheimer’s disease. *IEEE Trans. Biomed. Eng.* 62, 1132–1140. <https://doi.org/10.1109/TBME.2014.2372011>
- Lu, D., Popuri, K., Ding, G.W., Balachandar, R., Beg, M.F., Alzheimer’s Disease Neuroimaging Initiative, 2018. Multimodal and Multiscale Deep Neural Networks for the Early Diagnosis of Alzheimer’s Disease using structural MR and FDG-PET images. *Sci. Rep.* 8, 5697.
<https://doi.org/10.1038/s41598-018-22871-z>

- Lu, D., Weng, Q., 2007. A survey of image classification methods and techniques for improving classification performance. *Int. J. Remote Sens.* 28, 823–870. <https://doi.org/10.1080/01431160600746456>
- Lundervold, A.S., Lundervold, A., 2018. An overview of deep learning in medical imaging focusing on MRI. *Z. Med. Phys.* <https://doi.org/10.1016/j.zemedi.2018.11.002>
- Maas, A.L., Hannun, A.Y., Ng, A.Y., 2013. Rectifier nonlinearities improve neural network acoustic models, in: *Proc. Icml.* p. 3.
- Madabhushi, A., Udupa, J.K., 2005. Interplay between intensity standardization and inhomogeneity correction in MR image processing. *IEEE Trans. Med. Imaging* 24, 561–576. <https://doi.org/10.1109/TMI.2004.843256>
- Mahanand, B.S., Suresh, S., Sundararajan, N., Aswatha Kumar, M., 2012. Identification of brain regions responsible for Alzheimer’s disease using a Self-adaptive Resource Allocation Network. *Neural Netw.* 32, 313–322. <https://doi.org/10.1016/j.neunet.2012.02.035>
- Maitra, M., Chatterjee, A., 2006. A Slantlet transform based intelligent system for magnetic resonance brain image classification. *Biomed. Signal Process. Control* 1, 299–306. <https://doi.org/10.1016/j.bspc.2006.12.001>
- Marcus, D.S., Wang, T.H., Parker, J., Csernansky, J.G., Morris, J.C., Buckner, R.L., 2007. Open Access Series of Imaging Studies (OASIS): cross-sectional MRI data in young, middle aged, nondemented, and demented older adults. *J. Cogn. Neurosci.* 19, 1498–1507. <https://doi.org/10.1162/jocn.2007.19.9.1498>
- Mathew, N.A., Vivek, R.S., Anurenjan, P.R., 2018. Early Diagnosis of Alzheimer’s Disease from MRI Images Using PNN, in: 2018 International CET Conference on Control, Communication, and Computing (IC4). pp. 161–164. <https://doi.org/10.1109/CETIC4.2018.8530910>
- McKhann, G., Drachman, D., Folstein, M., Katzman, R., Price, D., Stadlan, E.M., 1984. Clinical diagnosis of Alzheimer’s disease Report of the NINCDS-ADRDA Work Group* under the auspices of Department of Health and Human Services Task Force on Alzheimer’s Disease. *Neurology* 34, 939–939.
- Mostapha, M., Kim, S., Wu, G., Zsembik, L., Pizer, S., Styner, M., 2018. NON-EUCLIDEAN, CONVOLUTIONAL LEARNING ON CORTICAL BRAIN SURFACES. *Proc. IEEE Int. Symp. Biomed. Imaging 2018*, 527–530. <https://doi.org/10.1109/ISBI.2018.8363631>
- Nair, V., Hinton, G.E., 2010. Rectified linear units improve restricted boltzmann machines, in: *Proceedings of the 27th International Conference on Machine Learning (ICML-10)*. pp. 807–814.
- Ning, K., Chen, B., Sun, F., Hobel, Z., Zhao, L., Matloff, W., Alzheimer’s Disease Neuroimaging Initiative, Toga, A.W., 2018. Classifying Alzheimer’s disease with brain imaging and genetic data using a neural network framework. *Neurobiol. Aging* 68, 151–158. <https://doi.org/10.1016/j.neurobiolaging.2018.04.009>
- Oliveira, F.P.M., Tavares, J.M.R.S., 2014. Medical image registration: a review. *Comput. Methods Biomech. Biomed. Engin.* 17, 73–93. <https://doi.org/10.1080/10255842.2012.670855>
- Ortiz, A., Munilla, J., Górriz, J.M., Ramírez, J., 2016. Ensembles of Deep Learning Architectures for the Early Diagnosis of the Alzheimer’s Disease. *Int. J. Neural Syst.* 26, 1650025. <https://doi.org/10.1142/S0129065716500258>
- Panigrahi, A., Chen, Y., -C. Jay Kuo, C., 2018. ANALYSIS ON GRADIENT PROPAGATION IN BATCH NORMALIZED RESIDUAL NETWORKS.
- Parisot, S., Ktena, S.I., Ferrante, E., Lee, M., Guerrero, R., Glocker, B., Rueckert, D., 2018. Disease prediction using graph convolutional networks: Application to Autism Spectrum Disorder and Alzheimer’s disease. *Med. Image Anal.* 48, 117–130. <https://doi.org/10.1016/j.media.2018.06.001>
- Paszke, A., Gross, S., Chintala, S., Chanan, G., Yang, E., DeVito, Z., Lin, Z., Desmaison, A., Antiga, L., Lerer, A., 2017. Automatic differentiation in PyTorch.
- Pedregosa, F., Varoquaux, G., Gramfort, A., Michel, V., Thirion, B., Grisel, O., Blondel, M., Prettenhofer, P., Weiss, R., Dubourg, V., Vanderplas, J., Passos, A., Cournapeau, D., Brucher, M., Perrot, M., Duchesnay, É., 2011. Scikit-learn: Machine Learning in Python. *J. Mach. Learn. Res.* 12, 2825–2830.
- Perez, L., Wang, J., 2017. The Effectiveness of Data Augmentation in Image Classification using Deep Learning. *arXiv [cs.CV]*.
- Petersen, R.C., Aisen, P.S., Beckett, L.A., Donohue, M.C., Gamst, A.C., Harvey, D.J., Jack, C.R., Jr, Jagust, W.J., Shaw, L.M., Toga, A.W., Trojanowski, J.Q., Weiner, M.W., 2010. Alzheimer’s Disease Neuroimaging Initiative (ADNI): clinical characterization. *Neurology* 74, 201–209. <https://doi.org/10.1212/WNL.0b013e3181cb3e25>

- Poldrack, R.A., Baker, C.I., Durnez, J., Gorgolewski, K.J., Matthews, P.M., Munafò, M.R., Nichols, T.E., Poline, J.-B., Vul, E., Yarkoni, T., 2017. Scanning the horizon: towards transparent and reproducible neuroimaging research. *Nat. Rev. Neurosci.* 18, 115–126. <https://doi.org/10.1038/nrn.2016.167>
- Prechelt, L., 2012. Early Stopping — But When?, in: Montavon, G., Orr, G.B., Müller, K.-R. (Eds.), *Neural Networks: Tricks of the Trade: Second Edition*. Springer Berlin Heidelberg, Berlin, Heidelberg, pp. 53–67. https://doi.org/10.1007/978-3-642-35289-8_5
- Qiu, S., Chang, G.H., Panagia, M., Gopal, D.M., Au, R., Kolachalama, V.B., 2018. Fusion of deep learning models of MRI scans, Mini-Mental State Examination, and logical memory test enhances diagnosis of mild cognitive impairment. *Alzheimer's & Dementia: Diagnosis, Assessment & Disease Monitoring* 10, 737–749. <https://doi.org/10.1016/j.dadm.2018.08.013>
- Raschka, S., 2015. *Python Machine Learning*. Packt Publishing Ltd.
- Rathore, S., Habes, M., Iftikhar, M.A., Shacklett, A., Davatzikos, C., 2017. A review on neuroimaging-based classification studies and associated feature extraction methods for Alzheimer's disease and its prodromal stages. *Neuroimage* 155, 530–548. <https://doi.org/10.1016/j.neuroimage.2017.03.057>
- Raut, A., Dalal, V., 2017. A machine learning based approach for detection of alzheimer's disease using analysis of hippocampus region from MRI scan, in: 2017 International Conference on Computing Methodologies and Communication (ICCMC). pp. 236–242. <https://doi.org/10.1109/ICCMC.2017.8282683>
- Razzak, M.I., Naz, S., Zaib, A., 2018. Deep Learning for Medical Image Processing: Overview, Challenges and the Future, in: Dey, N., Ashour, A.S., Borra, S. (Eds.), *Classification in BioApps: Automation of Decision Making*. Springer International Publishing, Cham, pp. 323–350. https://doi.org/10.1007/978-3-319-65981-7_12
- Ripley, B.D., 1996. *Pattern Recognition and Neural Networks* by Brian D. Ripley. Cambridge University Press. <https://doi.org/10.1017/CBO9780511812651>
- Routier, A., Guillon, J., Burgos, N., 2018. Clinica: an open source software platform for reproducible clinical neuroscience studies. Annual meeting of the.
- Salvatore, C., Cerasa, A., Battista, P., Gilardi, M.C., Quattrone, A., Castiglioni, I., Alzheimer's Disease Neuroimaging Initiative, 2015. Magnetic resonance imaging biomarkers for the early diagnosis of Alzheimer's disease: a machine learning approach. *Front. Neurosci.* 9, 307. <https://doi.org/10.3389/fnins.2015.00307>
- Samper-González, J., Burgos, N., Bottani, S., Fontanella, S., Lu, P., Marcoux, A., Routier, A., Guillon, J., Bacci, M., Wen, J., Bertrand, A., Bertin, H., Habert, M.-O., Durrleman, S., Evgeniou, T., Colliot, O., Alzheimer's Disease Neuroimaging Initiative, Australian Imaging Biomarkers and Lifestyle flagship study of ageing, 2018. Reproducible evaluation of classification methods in Alzheimer's disease: Framework and application to MRI and PET data. *Neuroimage*. <https://doi.org/10.1016/j.neuroimage.2018.08.042>
- Sarle, W.S., 1997. Neural Network FAQ, part 1 of 7. Introduction, periodic posting to the Usenet newsgroup comp. ai. neural-nets URL: <ftp://ftp.sas.com/pub/neural/FAQ.html>.
- Scherer, D., Müller, A., Behnke, S., 2010. Evaluation of Pooling Operations in Convolutional Architectures for Object Recognition, in: *Artificial Neural Networks – ICANN 2010*. Springer Berlin Heidelberg, pp. 92–101. https://doi.org/10.1007/978-3-642-15825-4_10
- Schuff, N., Woerner, N., Boreta, L., Kornfield, T., Shaw, L.M., Trojanowski, J.Q., Thompson, P.M., Jack, C.R., Jr, Weiner, M.W., Alzheimer's Disease Neuroimaging Initiative, 2009. MRI of hippocampal volume loss in early Alzheimer's disease in relation to ApoE genotype and biomarkers. *Brain* 132, 1067–1077. <https://doi.org/10.1093/brain/awp007>
- Senanayake, U., Sowmya, A., Dawes, L., 2018. Deep fusion pipeline for mild cognitive impairment diagnosis, in: 2018 IEEE 15th International Symposium on Biomedical Imaging (ISBI 2018). pp. 1394–1997. <https://doi.org/10.1109/ISBI.2018.8363832>
- Shams-Baboli, A., Ezoji, M., 2017. A Zernike moment based method for classification of Alzheimer's disease from structural MRI, in: 2017 3rd International Conference on Pattern Recognition and Image Analysis (IPRIA). pp. 38–43. <https://doi.org/10.1109/IPRIA.2017.7983061>
- Shattuck, D.W., Sandor-Leahy, S.R., Schaper, K.A., Rottenberg, D.A., Leahy, R.M., 2001. Magnetic resonance image tissue classification using a partial volume model. *Neuroimage* 13, 856–876. <https://doi.org/10.1006/nimg.2000.0730>

- Shen, T., Jiang, J., Li, Y., Wu, P., Zuo, C., Yan, Z., 2018. Decision Supporting Model for One-year Conversion Probability from MCI to AD using CNN and SVM, in: 2018 40th Annual International Conference of the IEEE Engineering in Medicine and Biology Society (EMBC). pp. 738–741. <https://doi.org/10.1109/EMBC.2018.8512398>
- Shi, J., Zheng, X., Li, Y., Zhang, Q., Ying, S., 2018. Multimodal Neuroimaging Feature Learning With Multimodal Stacked Deep Polynomial Networks for Diagnosis of Alzheimer’s Disease. *IEEE J Biomed Health Inform* 22, 173–183. <https://doi.org/10.1109/JBHI.2017.2655720>
- Shmulev, Y., Belyaev, M., The Alzheimer’s Disease Neuroimaging Initiative, 2018. Predicting Conversion of Mild Cognitive Impairments to Alzheimer’s Disease and Exploring Impact of Neuroimaging: Second International Workshop, GRAIL 2018 and First International Workshop, Beyond MIC 2018, Held in Conjunction with MICCAI 2018, Granada, Spain, September 20, 2018, Proceedings, in: Stoyanov, D., Taylor, Z., Ferrante, E., Dalca, A.V., Martel, A., Maier-Hein, L., Parisot, S., Sotiras, A., Papiez, B., Sabuncu, M.R., Shen, L. (Eds.), *Graphs in Biomedical Image Analysis and Integrating Medical Imaging and Non-Imaging Modalities*, Lecture Notes in Computer Science. Springer International Publishing, Cham, pp. 83–91. https://doi.org/10.1007/978-3-030-00689-1_9
- Simonyan, K., Zisserman, A., 2014. Very Deep Convolutional Networks for Large-Scale Image Recognition. *arXiv [cs.CV]*.
- Sled, J.G., Zijdenbos, A.P., Evans, A.C., 1998. A nonparametric method for automatic correction of intensity nonuniformity in MRI data. *IEEE Trans. Med. Imaging* 17, 87–97. <https://doi.org/10.1109/42.668698>
- Smith, S.M., 2002. Fast robust automated brain extraction. *Hum. Brain Mapp.* 17, 143–155. <https://doi.org/10.1002/hbm.10062>
- Sonnenburg, S., Braun, M.L., Ong, C.S., Bengio, S., Bottou, L., Holmes, G., LeCun, Y., Müller, K.-R., Pereira, F., Rasmussen, C.E., Rätsch, G., Schölkopf, B., Smola, A., Vincent, P., Weston, J., Williamson, R., 2007. The Need for Open Source Software in Machine Learning. *J. Mach. Learn. Res.* 8, 2443–2466.
- Spasov, S.E., Passamonti, L., Duggento, A., Lio, P., Toschi, N., 2018. A Multi-modal Convolutional Neural Network Framework for the Prediction of Alzheimer’s Disease. *Conf. Proc. IEEE Eng. Med. Biol. Soc.* 2018, 1271–1274. <https://doi.org/10.1109/EMBC.2018.8512468>
- Srivastava, N., Hinton, G., Krizhevsky, A., Sutskever, I., Salakhutdinov, R., 2014. Dropout: a simple way to prevent neural networks from overfitting. *J. Mach. Learn. Res.* 15, 1929–1958.
- Stodden, V., Leisch, F., Peng, R.D., 2014. *Implementing Reproducible Research*. CRC Press.
- Suk, H.-I., Lee, S.-W., Shen, D., Alzheimer’s Disease Neuroimaging Initiative, 2017. Deep ensemble learning of sparse regression models for brain disease diagnosis. *Med. Image Anal.* 37, 101–113. <https://doi.org/10.1016/j.media.2017.01.008>
- Suk, H.-I., Lee, S.-W., Shen, D., Alzheimer’s Disease Neuroimaging Initiative, 2015. Latent feature representation with stacked auto-encoder for AD/MCI diagnosis. *Brain Struct. Funct.* 220, 841–859. <https://doi.org/10.1007/s00429-013-0687-3>
- Suk, H.-I., Lee, S.-W., Shen, D., Alzheimer’s Disease Neuroimaging Initiative, 2014. Hierarchical feature representation and multimodal fusion with deep learning for AD/MCI diagnosis. *Neuroimage* 101, 569–582. <https://doi.org/10.1016/j.neuroimage.2014.06.077>
- Szegedy, C., Liu, W., Jia, Y., Sermanet, P., Reed, S., Anguelov, D., Erhan, D., Vanhoucke, V., Rabinovich, A., 2015. Going deeper with convolutions, in: *Proceedings of the IEEE Conference on Computer Vision and Pattern Recognition*. pp. 1–9.
- Taqi, A.M., Awad, A., Al-Azzo, F., Milanova, M., 2018. The Impact of Multi-Optimizers and Data Augmentation on TensorFlow Convolutional Neural Network Performance, in: *2018 IEEE Conference on Multimedia Information Processing and Retrieval (MIPR)*. pp. 140–145. <https://doi.org/10.1109/MIPR.2018.00032>
- Thung, K.-H., Yap, P.-T., Shen, D., 2017. Multi-stage Diagnosis of Alzheimer’s Disease with Incomplete Multimodal Data via Multi-task Deep Learning. *Deep Learn Med Image Anal Multimodal Learn Clin Decis Support (2017)* 10553, 160–168. https://doi.org/10.1007/978-3-319-67558-9_19
- Tustison, N.J., Avants, B.B., Cook, P.A., Zheng, Y., Egan, A., Yushkevich, P.A., Gee, J.C., 2010. N4ITK: improved N3 bias correction. *IEEE Trans. Med. Imaging* 29, 1310–1320. <https://doi.org/10.1109/TMI.2010.2046908>
- Uchida, S., 2013. Image processing and recognition for biological images. *Dev. Growth Differ.* 55, 523–549. <https://doi.org/10.1111/dgd.12054>

- Valliani, A., Soni, A., 2017. Deep Residual Nets for Improved Alzheimer's Diagnosis, in: Proceedings of the 8th ACM International Conference on Bioinformatics, Computational Biology, and Health Informatics. ACM, pp. 615–615. <https://doi.org/10.1145/3107411.3108224>
- Vanschoren, J., van Rijn, J.N., Bischl, B., Torgo, L., 2014. OpenML: Networked Science in Machine Learning. *SIGKDD Explor. Newsl.* 15, 49–60. <https://doi.org/10.1145/2641190.2641198>
- Vovk, U., Pernus, F., Likar, B., 2007. A review of methods for correction of intensity inhomogeneity in MRI. *IEEE Trans. Med. Imaging* 26, 405–421. <https://doi.org/10.1109/TMI.2006.891486>
- Vu, T.-D., Ho, N.-H., Yang, H.-J., Kim, J., Song, H.-C., 2018. Non-white matter tissue extraction and deep convolutional neural network for Alzheimer's disease detection. *Soft Comput* 22, 6825–6833. <https://doi.org/10.1007/s00500-018-3421-5>
- Vu, T.D., Yang, H.-J., Nguyen, V.Q., Oh, A.-R., Kim, M.-S., 2017. Multimodal learning using Convolution Neural Network and Sparse Autoencoder, in: 2017 IEEE International Conference on Big Data and Smart Computing (BigComp). pp. 309–312. <https://doi.org/10.1109/BIGCOMP.2017.7881683>
- Wang, H., Shen, Y., Wang, S., Xiao, T., Deng, L., Wang, X., Zhao, X., 2019. Ensemble of 3D densely connected convolutional network for diagnosis of mild cognitive impairment and Alzheimer's disease. *Neurocomputing* 333, 145–156. <https://doi.org/10.1016/j.neucom.2018.12.018>
- Wang, S.-H., Phillips, P., Sui, Y., Liu, B., Yang, M., Cheng, H., 2018. Classification of Alzheimer's Disease Based on Eight-Layer Convolutional Neural Network with Leaky Rectified Linear Unit and Max Pooling. *J. Med. Syst.* 42, 85. <https://doi.org/10.1007/s10916-018-0932-7>
- Wang, S., Shen, Y., Chen, W., Xiao, T., Hu, J., 2017. Automatic Recognition of Mild Cognitive Impairment from MRI Images Using Expedited Convolutional Neural Networks, in: Artificial Neural Networks and Machine Learning – ICANN 2017. Springer International Publishing, pp. 373–380. https://doi.org/10.1007/978-3-319-68600-4_43
- Wang, X., Cai, W., Shen, D., Huang, H., 2018. Temporal Correlation Structure Learning for MCI Conversion Prediction: 21st International Conference, Granada, Spain, September 16-20, 2018, Proceedings, Part III, in: Frangi, A.F., Schnabel, J.A., Davatzikos, C., Alberola-López, C., Fichtinger, G. (Eds.), Medical Image Computing and Computer Assisted Intervention – MICCAI 2018, Lecture Notes in Computer Science. Springer International Publishing, Cham, pp. 446–454. https://doi.org/10.1007/978-3-030-00931-1_51
- Wen, D., Wei, Z., Zhou, Y., Li, G., Zhang, X., Han, W., 2018. Deep Learning Methods to Process fMRI Data and Their Application in the Diagnosis of Cognitive Impairment: A Brief Overview and Our Opinion. *Front. Neuroinform.* 12, 23. <https://doi.org/10.3389/fninf.2018.00023>
- Wen, J., Samper-Gonzalez, J., Bottani, S., Routier, A., Burgos, N., Jacquemont, T., Fontanella, S., Durrleman, S., Epelbaum, S., Bertrand, A., Colliot, O., 2018. Reproducible evaluation of diffusion MRI features for automatic classification of patients with Alzheimers disease. *arXiv [q-bio.QM]*.
- Wu, C., Guo, S., Hong, Y., Xiao, B., Wu, Y., Zhang, Q., Alzheimer's Disease Neuroimaging Initiative, 2018. Discrimination and conversion prediction of mild cognitive impairment using convolutional neural networks. *Quant. Imaging Med. Surg.* 8, 992–1003. <https://doi.org/10.21037/qims.2018.10.17>
- Yann, L., 1987. Modeles connexionnistes de l'apprentissage. PhD thesis, These de Doctorat, Universite Paris 6.
- Yao, Y., Rosasco, L., Caponnetto, A., 2007. On Early Stopping in Gradient Descent Learning. *Constr. Approx.* 26, 289–315. <https://doi.org/10.1007/s00365-006-0663-2>
- Zhang, T., Yu, B., 2005. Boosting with early stopping: Convergence and consistency. *Ann. Stat.* 33, 1538–1579. <https://doi.org/10.1214/009053605000000255>
- Zhang, Y., Wang, S., Sui, Y., Yang, M., Liu, B., Cheng, H., Sun, J., Jia, W., Phillips, P., Gorriz, J.M., 2018. Multivariate Approach for Alzheimer's Disease Detection Using Stationary Wavelet Entropy and Predator-Prey Particle Swarm Optimization. *J. Alzheimers. Dis.* 65, 855–869. <https://doi.org/10.3233/JAD-170069>
- Zhou, T., Thung, K.-H., Zhu, X., Shen, D., 2019. Effective feature learning and fusion of multimodality data using stage-wise deep neural network for dementia diagnosis. *Hum. Brain Mapp.* 40, 1001–1016. <https://doi.org/10.1002/hbm.24428>
- Zhou, T., Thung, K.-H., Zhu, X., Shen, D., 2017. Feature Learning and Fusion of Multimodality Neuroimaging and Genetic Data for Multi-status Dementia Diagnosis. *Mach Learn Med Imaging* 10541,

Table 5. Summary of all the classification experiments and validation results in our analyses.

MinMax: for CNNs, intensity rescaling was done based on min and max values, resulting all values to be in the range of [0, 1]; SPM-based: the intensity rescaling was performed with SPM; AE: autoencoder. For DL models, sMCI vs pMCI tasks were done as follows: the weights and biases of the model learnt on the source task (AD vs CN) were transferred to a new model fine-tuned on the target task (sMCI vs pMCI). For SVM, the sMCI vs pMCI was done either training directly on sMCI vs pMCI or using training on AD vs CN and applying the trained model to sMCI vs pMCI.

Classification architectures	Training data	Image preprocessing	Intensity rescaling	Data split	Training approach	Transfer learning	Task	Validation accuracy
3D subject-level CNN	Baseline	Minimal	None	subject-level	single-CNN	None	AD vs CN	0.50 ± 0.00 [0.50, 0.50, 0.50, 0.50, 0.50]
		MinMax						0.77 ± 0.08 [0.78, 0.87, 0.83, 0.75, 0.63]
	Longitudinal	Minimal	MinMax	subject-level	single-CNN	AE pre-train		0.78 ± 0.05 [0.79, 0.83, 0.82, 0.79, 0.68]
		Extensive						0.85 ± 0.03 [0.89, 0.87, 0.86, 0.82, 0.82]
	Baseline	Minimal					sMCI vs pMCI	0.74 ± 0.03 [0.75, 0.77, 0.70, 0.76, 0.72]
	Baseline							0.74 ± 0.03 [0.72, 0.76, 0.72, 0.78, 0.71]
3D ROI-based CNN	Baseline	Minimal	MinMax	subject-level	single-CNN	AE pre-train	AD vs CN	0.86 ± 0.03 [0.84, 0.89, 0.86, 0.88, 0.82]
							sMCI vs pMCI	0.80 ± 0.03 [0.84, 0.79, 0.75, 0.79, 0.82]
	Longitudinal						AD vs CN	0.85 ± 0.02 [0.84, 0.87, 0.86, 0.88, 0.82]

							sMCI vs pMCI	0.79 ± 0.03 [0.82, 0.78, 0.73, 0.79, 0.81]
3D patch-level CNN	Baseline	Minimal	MinMax	subject-level	single-CNN	AE pre-train	AD vs CN	0.72 ± 0.09 [0.75, 0.83, 0.75, 0.73, 0.56]
	Longitudinal							0.72 ± 0.06 [0.77, 0.74, 0.77, 0.69, 0.61]
	Baseline				multi-CNN		AD vs CN	0.81 ± 0.03 [0.85, 0.81, 0.75, 0.79, 0.83]
	Baseline						sMCI vs pMCI	0.76 ± 0.04 [0.80, 0.75, 0.68, 0.79, 0.78]
	Longitudinal						AD vs CN	0.79 ± 0.02 [0.81, 0.75, 0.80, 0.80, 0.80]
	Longitudinal						sMCI vs pMCI	0.76 ± 0.03 [0.78, 0.77, 0.71, 0.78, 0.76]
2D slice-level CNN	Baseline	Minimal	MinMax	subject-level	single-CNN	ImageNet pre-train	AD vs CN	0.79 ± 0.04 [0.82, 0.83, 0.72, 0.82, 0.76]
	Longitudinal							0.79 ± 0.05 [0.79, 0.85, 0.80, 0.82, 0.70]
	Baseline			slice-level (data leakage)				1.00 ± 0 [1.00, 1.00, 1.00, 1.00, 1.00]
SVM	Baseline	DartelGM	SPM-bas ed	subject-level	None	None	AD vs CN	0.85 ± 0.02 [0.85, 0.88, 0.83, 0.86, 0.84]
							sMCI vs pMCI (trained on sMCI vs pMCI)	0.69 ± 0.02 [0.71, 0.70, 0.66, 0.67, 0.72]
							sMCI vs pMCI (trained on AD vs CN)	0.72 ± 0.04 [0.67, 0.78, 0.70, 0.76, 0.68]

		None	AD vs CN	0.85 ± 0.01 [0.87, 0.85, 0.84, 0.86, 0.85]
Longitudinal			sMCI vs pMCI (trained on sMCI vs pMCI)	0.68 ± 0.07 [0.76, 0.76, 0.59, 0.63, 0.65]
			sMCI vs pMCI (trained on AD vs CN)	0.69 ± 0.03 [0.66, 0.73, 0.70, 0.73, 0.65]

Table 6. Summary of the results of the three test datasets in our analyses.

MinMax: for CNNs, intensity rescaling was done based on min and max values, resulting all values to be in the range of [0, 1]; SPM-based: the intensity rescaling was performed with SPM; AE: autoencoder.

Classification architectures	Training data	Image preprocessing	Intensity rescaling	Data split	Training approach	Transfer learning	Task	Validation accuracy	ADNI test accuracy	AIBL test accuracy	OASIS test accuracy
3D subject-level CNN	Baseline	Minimal	MinMax	subject-level	single-CNN	AE pre-train	AD vs CN	0.78 ± 0.05			
	Longitudinal							0.85 ± 0.03			
	Baseline						sMCI vs pMCI	0.75 ± 0.02			
	Longitudinal							0.74 ± 0.03			
3D ROI-based CNN	Baseline	Minimal	MinMax	subject-level	single-CNN	AE pre-train	AD vs CN	0.86 ± 0.03			
	Longitudinal										
	Baseline						sMCI vs pMCI	0.80 ± 0.03			
	Longitudinal						AD vs CN	0.85 ± 0.02			
3D patch-level CNN	Baseline	Minimal	MinMax	subject-level	multi-CNN	AE pre-train	AD vs CN	0.81 ± 0.03			
	Longitudinal										
	Baseline						sMCI vs pMCI	0.76 ± 0.04			
	Longitudinal						AD vs CN	0.79 ± 0.02			
3D patch-level CNN	Baseline	Minimal	MinMax	subject-level	multi-CNN	AE pre-train	sMCI vs pMCI	0.76 ± 0.03			
	Longitudinal										

2D slice-level CNN	Baseline	Minimal	MinMax	subject-level	single-CNN	ImageNet pre-train	AD vs CN	0.79 ± 0.04
	Longitudinal							0.79 ± 0.05
	Baseline			slice-level (data leakage)				1.00 ± 0
SVM		DartelGM	SPM-based	subject-level	None	None	AD vs CN	0.85 ± 0.02
	Baseline						sMCI vs pMCI (trained on AD vs CN)	0.72 ± 0.04
							AD vs CN	0.85 ± 0.01
	Longitudinal						sMCI vs pMCI (trained on AD vs CN)	0.69 ± 0.03

Convolutional Neural Networks for Classification of Alzheimer's Disease: Overview and Reproducible Evaluation

Supplementary Material

Junhao Wen^{a,b,c,d,e}, Elina Thibeau--Sutre^{a,b,c,d,e}, Jorge Samper-González^{e,a,b,c,d}, Alexandre Routier^{e,a,b,c,d}, Simona Bottani^{e,a,b,c,d}, Stanley Durrleman^{e,a,b,c,d}, Ninon Burgos^{a,b,c,d,e}, Olivier Colliot^{a,b,c,d,e,f}, for the Alzheimer's Disease Neuroimaging Initiative and the Australian Imaging Biomarkers and Lifestyle flagship study of ageing

^a*Institut du Cerveau et de la Moelle épinière, ICM, F-75013, Paris, France*

^b*Sorbonne Université, F-75013, Paris, France*

^c*Inserm, U 1127, F-75013, Paris, France*

^d*CNRS, UMR 7225, F-75013, Paris, France*

^e*Inria, Aramis project-team, F-75013, Paris, France*

^f*AP-HP, Hôpital de la Pitié Salpêtrière, Department of Neurology and Neuroradiology, F-75013, Paris, France*

We present additional methodological explanations, tables and figures in this supplementary material. More specifically, we first present in detail the methodology of our literature review (eMethod 1). We then describe the datasets used in our study in eMethod 2. From eTable1 to eTable3, we present the architecture hyperparameters for the chosen models. The training hyperparameters for autoencoder pre-training and classification are shown in eTable 4 and eTable 5, respectively. Lastly, the monitoring of training process, including the display of the training/validation loss and accuracy, is presented from eFigure 1 to eFigure 4.

eMethod 1. Literature search method

eMethod 2. Datasets used in our study

eTable 1. Architecture for 3D subject-level CNN.

eTable 2. Architecture for 3D ROI-based and patch-level CNN

eTable 3. Architecture for 2D slice-level CNN

eTable 4. Training hyperparameters for classification experiments.

eTable 5. Training hyperparameters for autoencoder pretraining experiments.

eFigure 1. Training process monitoring for 3D subject-level CNN

eFigure 2. Training process monitoring for 3D ROI-based CNN

eFigure 3. Training process monitoring for 3D patch-level CNN

eFigure 4. Training process monitoring for 2D slice-level CNN

eMethod 1. Literature search methodology

We searched PubMed and Scopus for articles published up to the time of the search (15th of January 2019). Our request contains words linked to four different concepts: Alzheimer's disease, classification, deep learning and neuroimaging. The words matching these concepts were identified in the abstracts and titles of the articles of a first bibliography done on Google Scholar. In Scopus a restriction was added to remove the articles linked to electroencephalography that appeared with our query and were out of our scope. This restriction was not applied in PubMed as it concerns only a few articles (less than 10). The line of the query linked to the neuroimaging concept was extended to all fields, as some authors do not mention at all in the title, abstract or keywords the modalities that they employed.

Scopus query:

```
TITLE-ABS-KEY ( alzheimer's OR alzheimer OR "Mild Cognitive Impairment" )
AND
TITLE-ABS-KEY ( classification OR diagnosis OR identification OR detection OR recognition )
AND
TITLE-ABS-KEY ( cnn OR "Convolutional Network" OR "Deep Learning" OR "Neural Network" OR
autoencoder OR gan )
AND
ALL ( mri OR "Magnetic Resonance Imaging" OR "Structural Magnetic Resonance Imaging" OR
neuroimaging OR brain-imaging )
AND NOT
TITLE-ABS-KEY ( eeg OR eegs OR electroencephalogram OR electroencephalographic )
```

PubMed query:

```
(alzheimer's [Title/Abstract] OR alzheimer [Title/Abstract] OR "Mild Cognitive Impairment" [Title/Abstract]
)
AND
(cnn OR "Convolutional Network" [Title/Abstract] OR "Deep Learning" [Title/Abstract] OR "Neural
Network" [Title/Abstract] OR autoencoder [Title/Abstract] OR gan [Title/Abstract] )
AND
(classification [Title/Abstract] OR diagnosis [Title/Abstract] OR identification [Title/Abstract] OR detection
[Title/Abstract] OR recognition [Title/Abstract] )
AND
(mri OR "Magnetic Resonance Imaging" OR "Structural Magnetic Resonance Imaging" OR neuroimaging OR
brain-imaging)
```

391 records were found with Scopus and 80 records were found with PubMed. After merging the two sets and removing duplicates, 406 records were identified. Before filtering the result, we removed from this list 10 conference proceedings books and 1 non-english article. We finally ended with 395 records to filter.

Once identified, all records were filtered in a 3-step process. We selected the records based on the abstract, the type and the content.

1.1. Record screening based on abstract

During this step, the abstracts of the articles were read to keep only the methods corresponding to the following criteria:

- use of anatomical MRI (when the modality was specified),
- classification of AD stages, then we excluded papers using deep learning to preprocess, segment or complete data, as well as the classification of different diseases or classification of different symptoms in AD population (depression, ICD...),
- exclusion of animal models,
- exclusion of reviews.

We chose to exclude the 31 reviews of our set as none of them focused on our topic. We did not detail the reasons of the exclusion of the papers in the diagram as many papers cumulate several criteria of exclusion. After this screening phase, we were left with 124 records.

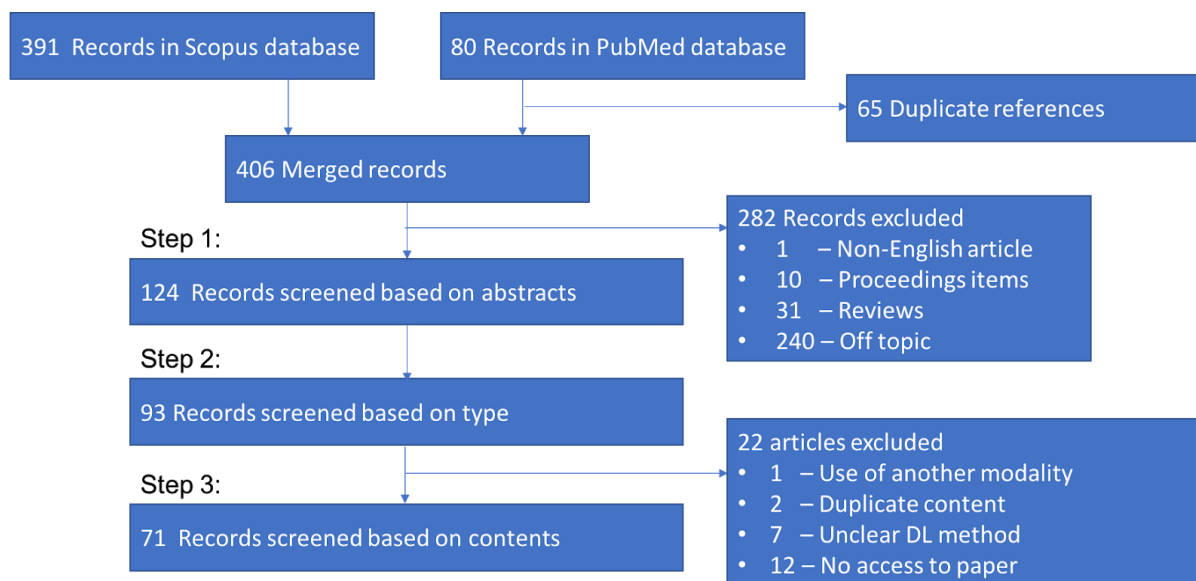
1.2. Record screening based on type

Our search on PubMed and Scopus comprises only peer-reviewed items. However, there is a different level of peer-review between conference papers and journal articles, hence we kept all journal articles and recent conference papers (published since 2017). We decided to not only restrict to journal articles because it would have reduced the number of items to 48. We decided to keep recent conference papers because we considered that if the older ones were not transformed into journal articles it may mean that their contributions were not sufficient. After this step, the set contained 93 items.

1.3. Record screening based on content

This step was mainly used to sort the papers between the different sections of our state-of-the-art. We detected in this way papers that were out of the scope of our review (longitudinal and multimodal studies, deep learning techniques other than CNN). We excluded only 22 papers because of i) use of another modality (1 paper); ii) duplicate content (2 papers); iii) lack of explanation on the method employed (7 papers); iv) no access to the content (12 papers). This step was reviewed by another member of the team to confirm the exclusions. In the end, our search resulted in 71 conference and journal articles, including 32 that are centered on our topic.

Diagram summarizing the bibliographic methodology



eMethod 2. Datasets used in our study

Part of the data used in the preparation of this article were obtained from the Alzheimer's Disease Neuroimaging Initiative database (adni.loni.usc.edu). The ADNI was launched in 2003 as a public-private partnership, led by Principal Investigator Michael W. Weiner, MD. The primary goal of ADNI has been to test whether serial MRI, PET, other biological markers, and clinical and neuropsychological assessment can be combined to measure the progression of mild cognitive impairment (MCI) and early AD. Over 1,650 participants were recruited across North America during the three phases of the study (ADNI1, ADNI GO and ADNI2). Around 400 participants were diagnosed with AD, 900 with MCI and 350 were control subjects. Three main criteria were used to classify the subjects (Petersen et al. 2010). The normal subjects had no memory complaints, while the subjects with MCI and AD both had to have complaints. CN and MCI subjects had a mini-mental state examination (MMSE) score between 24 and 30 (inclusive), and AD subjects between 20 and 26 (inclusive). The CN subjects had a clinical dementia rating (CDR) score of 0, the MCI subjects of 0.5 with a mandatory requirement of the memory box score being 0.5 or greater, and the AD subjects of 0.5 or 1. The other criteria can be found in (Petersen et al. 2010).

We also used data collected by the AIBL study group. Similarly to ADNI, the Australian Imaging, Biomarker & Lifestyle Flagship Study of Ageing seeks to discover which biomarkers, cognitive characteristics, and health and lifestyle factors determine the development of AD. AIBL has enrolled 1100 participants and collected over 4.5 years worth of longitudinal data: 211 AD patients, 133 MCI patients and 768 comparable healthy controls. AIBL study methodology has been reported previously (Ellis et al. 2009; Ellis et al. 2010). Briefly, the MCI diagnoses were made according to a protocol based on the criteria of (Winblad et al. 2004) and the AD diagnoses on the NINCDS-ADRDA criteria (McKhann et al. 1984). Note that about half of the subjects diagnosed as healthy controls reported memory complaints (Ellis et al. 2009; Ellis et al. 2010).

Finally, we used data from the Open Access Series of Imaging Studies project whose aim is to make MRI datasets of the brain freely available to the scientific community. We focused on the "Cross-sectional MRI Data in Young, Middle Aged, Nondemented and Demented Older Adults" set (Marcus et al. 2007), which consists of a cross-sectional collection of 416 subjects aged 18 to 96. 100 of the included subjects over the age of 60 have been clinically diagnosed with very mild to moderate AD. The criteria used to evaluate the diagnosis was the CDR score. All participants with a CDR greater than 0 were diagnosed with probable AD. Note that there are no MCI subjects in OASIS.

eTable 1. Architecture hyperparameters for 3D subject-level CNN.

As the architecture depends on the size of the input, it slightly differs between the two types of preprocessing (i.e. “Minimal” or “Extensive”). This difference only affects the size of the input of the first FC layer (FC1). The output size of each layer is reported depending on the preprocessing used in the last two columns.

The padding size in convolutional layers has been set to 1 not to decrease the size of the convolutional layer outputs. Without any padding, the number of nodes at the end of the last convolutional layer is too small to reconstruct the image correctly using an autoencoder for the Extensive preprocessing.

The padding size in pooling layers depends on the input: columns of zeros are added along a dimension until the size along this dimension is a multiple of the stride size.

Layer	Filter size	Number of filters / neurons	Stride size	Padding size	Dropout rate	Output size (Minimal)	Output size (Extensive)
Conv1+BN+ReLU	3x3x3	8	1	1	--	8x169x208x179	8x121x145x121
MaxPool1	2x2x2	--	2	adaptive	--	8x85x104x90	8x61x73x61
Conv2+BN+ReLU	3x3x3	16	1	1	--	16x85x104x90	16x61x73x61
MaxPool2	2x2x2	--	2	adaptive	--	16x43x52x45	16x31x37x31
Conv3+BN+ReLU	3x3x3	32	1	1	--	32x43x52x45	32x31x37x31
MaxPool3	2x2x2	--	2	adaptive	--	32x22x26x23	32x16x19x16
Conv4+BN+ReLU	3x3x3	64	1	1	--	64x22x26x23	64x16x19x16
MaxPool4	2x2x2	--	2	adaptive	--	64x11x13x12	64x8x10x8
Conv5+BN+ReLU	3x3x3	128	1	1	--	128x11x13x12	128x8x10x8
MaxPool5	2x2x2	--	2	adaptive	--	128x6x7x6	128x4x5x4
Dropout	--	--	--	--	0.5	128x6x7x6	128x4x5x4
FC1	--	1300	--	--	--	1300	1300
FC2	--	50	--	--	--	50	50
FC3	--	2	--	--	--	2	2
Softmax	--	--	--	--	--	--	2

BN: batch normalization; Conv: convolutional layer; FC: fully connected; MaxPool: max pooling.

eTable 2. Architecture hyperparameters for 3D ROI-based and patch-level CNN.

The padding size in pooling layers depends on the input: columns of zeros are added along a dimension until the size along this dimension is a multiple of the stride size.

Layer	Filter size	Number of filters / neurons	Stride size	Padding size	Dropout rate	Output size
Conv1+BN+ReLU	3x3x3	15	1	0	--	15x48x48x48
MaxPool1	2x2x2	--	2	adaptive	--	15x24x24x24
Conv2+BN+ReLU	3x3x3	25	1	0	--	25x22x22x22
MaxPool2	2x2x2	--	2	adaptive	--	25x11x11x11
Conv3+BN+ReLU	3x3x3	50	1	0	--	50x9x9x9
MaxPool3	2x2x2	--	2	adaptive	--	50x5x5x5
Conv4+BN+ReLU	3x3x3	50	1	0	--	50x3x3x3
MaxPool4	2x2x2	--	2	adaptive	--	50x2x2x2
Dropout1	--	--	--	--	0.5	50x2x2x2
FC1	--	50	--	--	--	50
Dropout2	--	--	--	--	0.5	50
FC2	--	40	--	--	--	40
FC3	--	2	--	--	--	2
Softmax	--	--	--	--	--	2

BN: batch normalization; Conv: convolutional layer; FC: fully connected; MaxPool: max pooling.

eTable 3. Architecture hyperparameters for 2D slice-level CNN.

Table B explicits the architecture of our 2D slice-level CNN. Shortcuts are displayed with arrows and are adding the two feature maps linked together and applying ReLU to form a new feature map given to the following layer.

When shortcuts are linking feature maps of different sizes, the arrow is associated with a downsampling layer (see table A) applied to the largest feature map.

A. Characteristics of the downsampling layers

Layer	Filter size	Number of filters / neurons	Stride size	Padding size	Dropout rate
Conv8	1x1	128	2	0	--
Conv13	1x1	256	2	0	--
Conv18	1x1	512	2	0	--

B. Architecture of the 2D slice-level CNN (adaptation of the ResNet-18)

Layer	Filter size	Number of filters / neurons	Stride size	Padding size	Dropout rate	Output size
Conv1+BN+ReLU	7x7	64	2	3	--	64x112x112
MaxPool1	3x3	--	2	1	--	64x56x56
Conv2+BN+ReLU	3x3	64	1	1	--	64x56x56
Conv3+BN	3x3	64	1	1	--	64x56x56
Conv4+BN+ReLU	3x3	64	1	1	--	64x56x56
Conv5+BN	3x3	64	1	1	--	64x56x56
Conv6+BN+ReLU	3x3	128	2	1	--	128x28x28
Conv7+BN	3x3	128	1	1	--	128x28x28
Conv9+BN+ReLU	3x3	128	1	1	--	128x28x28
Conv10+BN	3x3	128	1	1	--	128x28x28
Conv11+BN+ReLU	3x3	256	2	1	--	256x14x14
Conv12+BN	3x3	256	1	1	--	256x14x14
Conv14+BN+ReLU	3x3	256	1	1	--	256x14x14
Conv15+BN	3x3	256	1	1	--	256x14x14
Conv16+BN+ReLU	3x3	512	2	1	--	512x7x7
Conv17+BN	3x3	512	1	1	--	512x7x7
Conv19+BN+ReLU	3x3	512	1	1	--	512x7x7
Conv20+BN	3x3	512	1	1	--	512x7x7
AveragePool1	7x7	--	1	0	--	512x1x1
FC1	--	1000	--	--	--	1000
Dropout	--	--	--	--	0.8	1000
FC2	--	2	--	--	--	2
Softmax	--	--	--	--	--	2

eTable 4. Training hyperparameters for classification experiments.

A summary of the experiments can be found in Table A. The corresponding hyperparameters are listed in Table B indicated by the experiments numbers.

Common hyperparameters for all experiments: optimizer: Adam; Adam parameters: betas=(0.9, 0.999), epsilon=1e-8; loss: cross entropy.

When transfer learning is applied, the corresponding experiment number is given between brackets and can be found in eTable 5 for AE pretraining (AE) and eTable 4 for cross-task transfer learning (CTT).

A. Summary of experiments performed

Experiment number	Classification architectures	Training data	Image preprocessing	Intensity rescaling	Data split	Training approach	Transfer learning	Task	
1	3D subject-level CNN	Baseline	Minimal	None	subject-level	single-CNN	None	AD vs CN	
2				MinMax					
3		Longitudinal	Minimal	MinMax	subject-level	single-CNN	AE (1)		
4							AE (1)		
5							AE (2)		
6		Baseline	Minimal	MinMax	subject-level	single-CNN	CTT (4)		sMCI vs pMCI
7							CTT (3)		
8	3D ROI-based CNN	Baseline	Minimal	MinMax	subject-level	single-CNN	AE (3)	AD vs CN	
9							CTT (8)		sMCI vs pMCI
10		Longitudinal	Minimal	MinMax	subject-level	single-CNN	AE (4)	AD vs CN	
11							CTT (10)		sMCI vs pMCI
12							AE (5)		
13	3D patch-level CNN	Baseline	Minimal	MinMax	subject-level	single-CNN	AE (6)	AD vs CN	
14							AE (7)		AD vs CN
15		Longitudinal	Minimal	MinMax	subject-level	multi-CNN	CTT (14)	sMCI vs pMCI	
16							AE (8)		AD vs CN
17							CTT (16)		
18	2D slice-level CNN	Baseline	Minimal	MinMax	subject-level	single-CNN	ImageNet pre-train	AD vs CN	
19							Longitudinal		
20		Baseline	Minimal	MinMax	slice-level (data leakage)	subject-level	single-CNN	ImageNet pre-train	AD vs CN

B. Hyperparameters corresponding to experiments described in Table A.

Approach	Experiment	Number of epochs	Learning rate	Batch size	Dropout rate	Weight decay	Patience
3D subject-level CNN	1	50	1e-4	12	0.5	1e-4	10
	2	50	1e-4	12	0.5	1e-4	10
	3	50	1e-4	12	0.5	1e-4	10
	4	50	1e-4	12	0.5	1e-4	5
	5	50	1e-4	12	0.5	1e-4	5
	6	50	1e-5	12	0.5	1e-4	10
	7	50	1e-5	12	0.5	1e-4	20
3D ROI-based CNN	8	200	1e-5	32	0.5	1e-4	10
	9	200	1e-5	32	0.5	1e-3	20
	10	200	1e-5	32	0.5	1e-4	10
	11	200	1e-5	32	0.5	1e-3	20
3D patch-level CNN	12	200	1e-5	32	0.5	1e-3	20
	13	200	1e-5	32	0.5	1e-3	20
	14	200	1e-5	32	0.5	1e-4	15
	15	200	1e-5	32	0.5	1e-3	20
	16	200	1e-5	32	0.5	1e-4	15
	17	200	1e-5	32	0.5	1e-3	20
2D slice-level CNN	18	50	1e-6	32	0.8	1e-4	15
	19	100	1e-6	32	0.8	1e-4	15
	20	50	1e-6	32	0.8	1e-4	15

eTable 5. Training hyperparameters for autoencoder pretraining experiments.

A summary of the experiments can be found in table A. The corresponding hyperparameters are listed in Table B using the same experiments numbers.

Common hyperparameters for all experiments: optimizer: Adam; Adam parameters: betas=(0.9, 0.999), epsilon=1e-8; loss: mean squared entropy loss; training data: AD + MCI + CN; data split: subject-level. The stopping criterion is the maximal number of epochs.

A. Summary of autoencoder pretraining experiments performed.

Experiment number	Classification architectures	Training data	Image preprocessing	Intensity rescaling	Training approach
1	3D subject-level CNN	Baseline	Minimal	MinMax	single-CNN
2			Extensive		
3	3D ROI-based CNN	Baseline	Minimal	MinMax	single-CNN
4		Longitudinal			
5	3D patch-level CNN	Baseline	Minimal	MinMax	single-CNN
6		Longitudinal			
7		Baseline			multi-CNN
8		Longitudinal			

B. Hyperparameters corresponding to autoencoder pretraining experiments described in Table A.

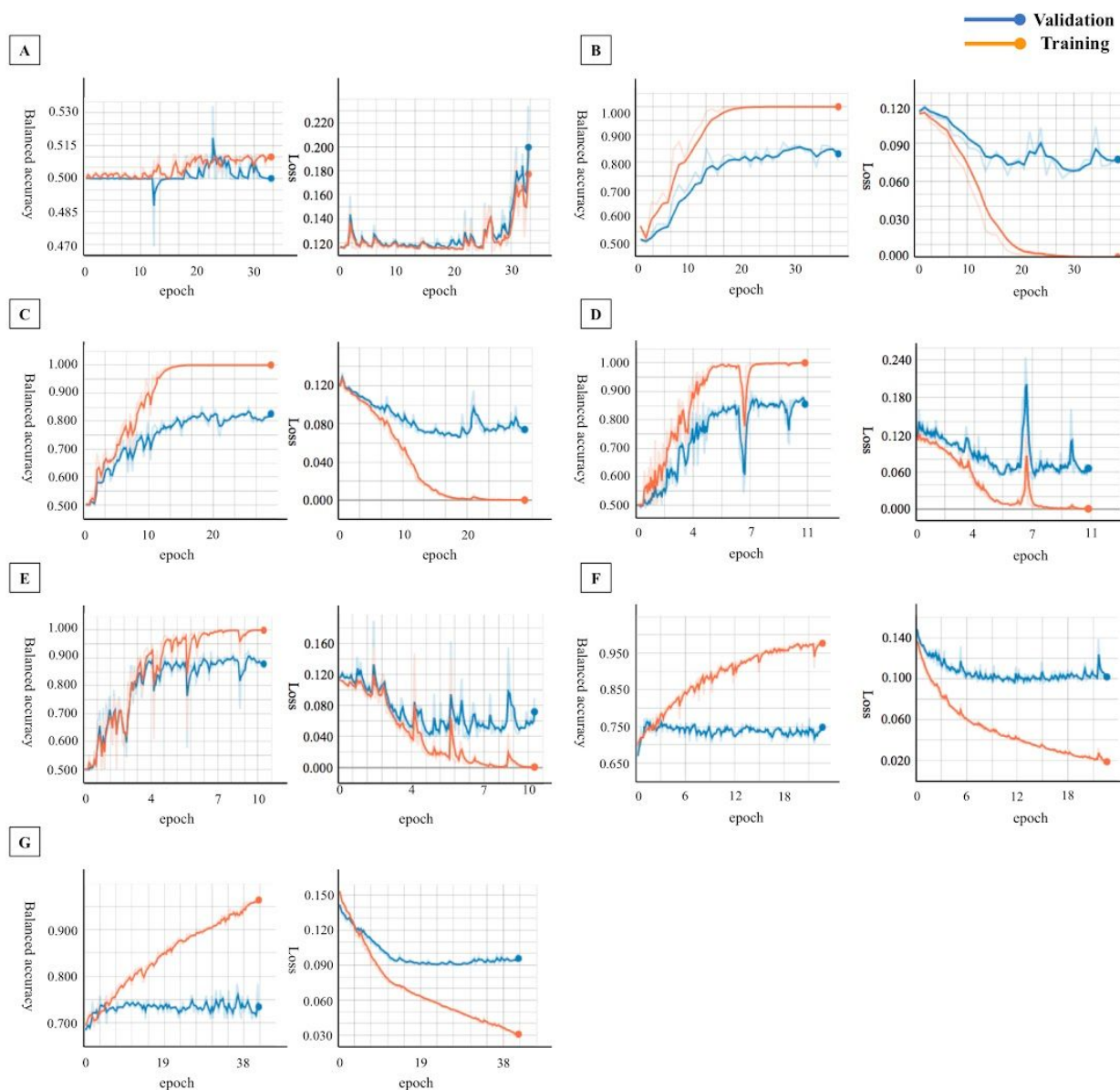
Approach	Experiment	Number of epochs	Learning rate	Batch size	Weight decay
3D subject-level CNN	1	50	1e-4	12	1e-4
	2	30	1e-4	12	1e-4
3D ROI-based CNN	3	200	1e-5	32	0
	4	100	1e-5	32	0
3D patch-level CNN	5	20	1e-5	32	0
	6	15	1e-5	32	0
	7	15	1e-5	32	0
	8	15	1e-5	32	0

eFigure 1. Training process monitoring for 3D subject-level CNN

Training and validation accuracy/loss during the training process were evaluated after the forward pass of 20 batches. The accuracy and loss curves were smoothed with a threshold (0.6).

For each plot a subfigure letter is used and the corresponding information on the experiment may be found in the table below or in eTable 4 according to the “Experiment number”.

Subfigure	Experiment number	Fold displayed	Epoch where training stopped	Epoch of the highest validation accuracy	Highest validation accuracy
A	1	2	32	22	0.50
B	2	2	37	27	0.87
C	3	2	28	28	0.83
D	4	2	11	10	0.87
E	5	2	10	9	0.91
F	6	2	23	1	0.77
G	7	2	42	37	0.77

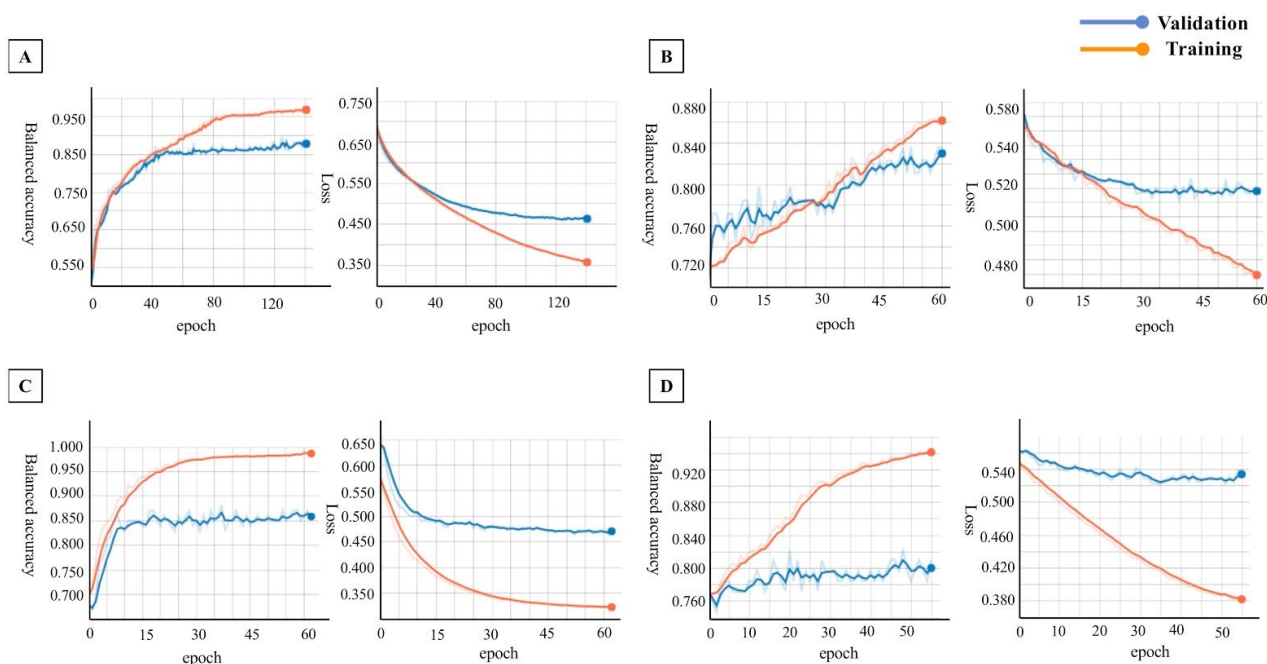


eFigure 2. Training process monitoring for 3D ROI-based CNN.

Training and validation accuracy/loss during the training process were evaluated after each epoch. The accuracy and loss curves were smoothed with a threshold (0.6).

For each plot a subfigure letter is used and the corresponding information on the experiment may be found in the table below or in eTable 4 according to the “Experiment number”.

Subfigure	Experiment number	Fold displayed	Epoch where training stopped	Epoch of the highest validation accuracy	Highest validation accuracy
A	8	2	141	125	0.89
B	9	1	60	60	0.84
C	10	3	89	51	0.88
D	11	3	55	48	0.82

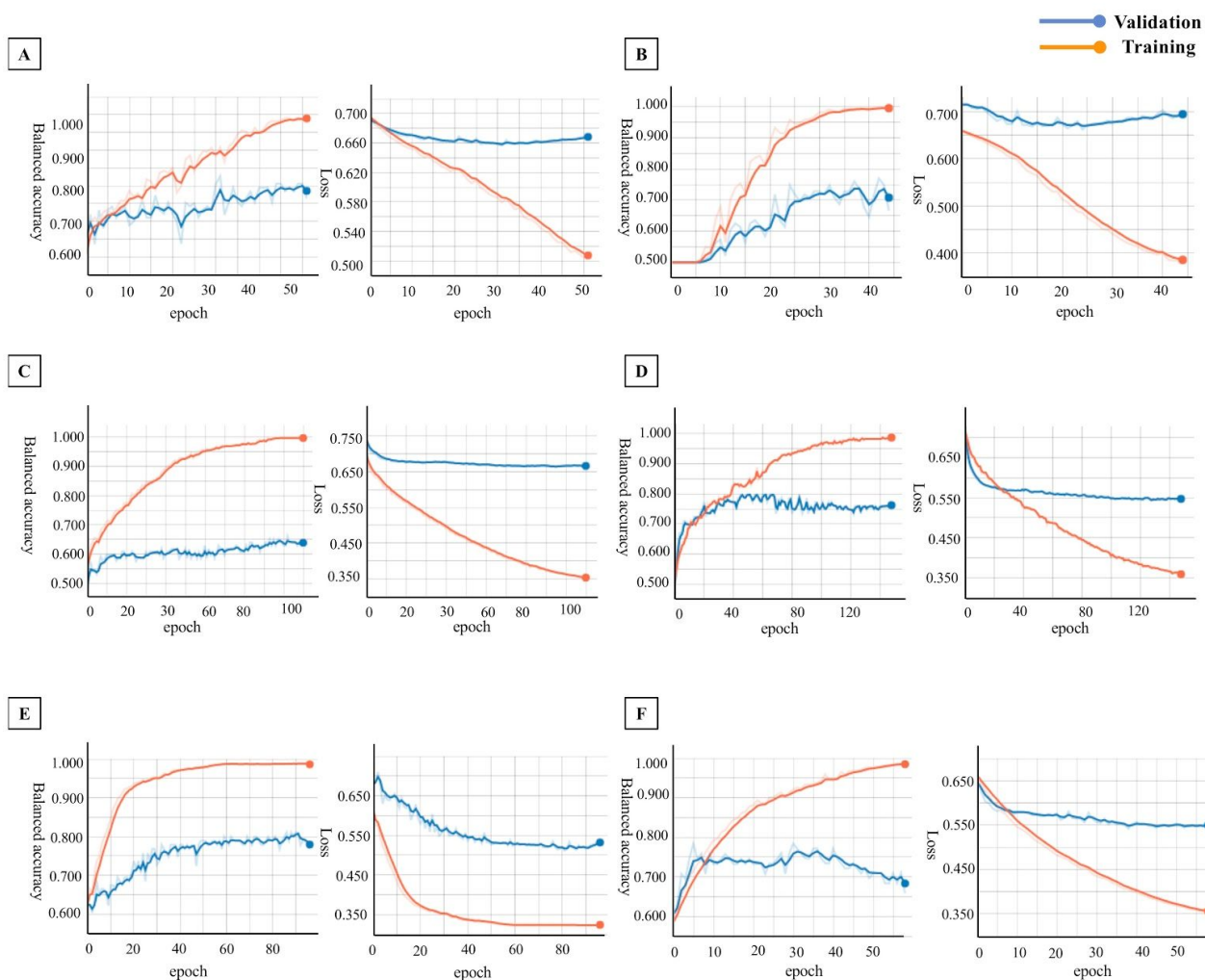


eFigure 3. Training process monitoring for 3D patch-level CNN

Training and validation accuracy/loss during the training process were evaluated after each epoch. The accuracy and loss curves were smoothed with a threshold (0.6).

For each plot a subfigure letter is used and the corresponding information on the experiment may be found in the table below or in eTable 4 according to the “Experiment number”. For multi-CNN experiments the CNN number is provided.

Subfigure	Experiment number	Fold displayed	CNN number	Epoch where training stopped	Epoch of the highest validation accuracy	Highest validation accuracy
A	12	2	--	51	31	0.83
B	13	2	--	51	31	0.83
C	14	1	5	110	110	0.85
D	15	1	19	148	46	0.80
E	16	1	29	96	86	0.81
F	17	1	19	58	30	0.78

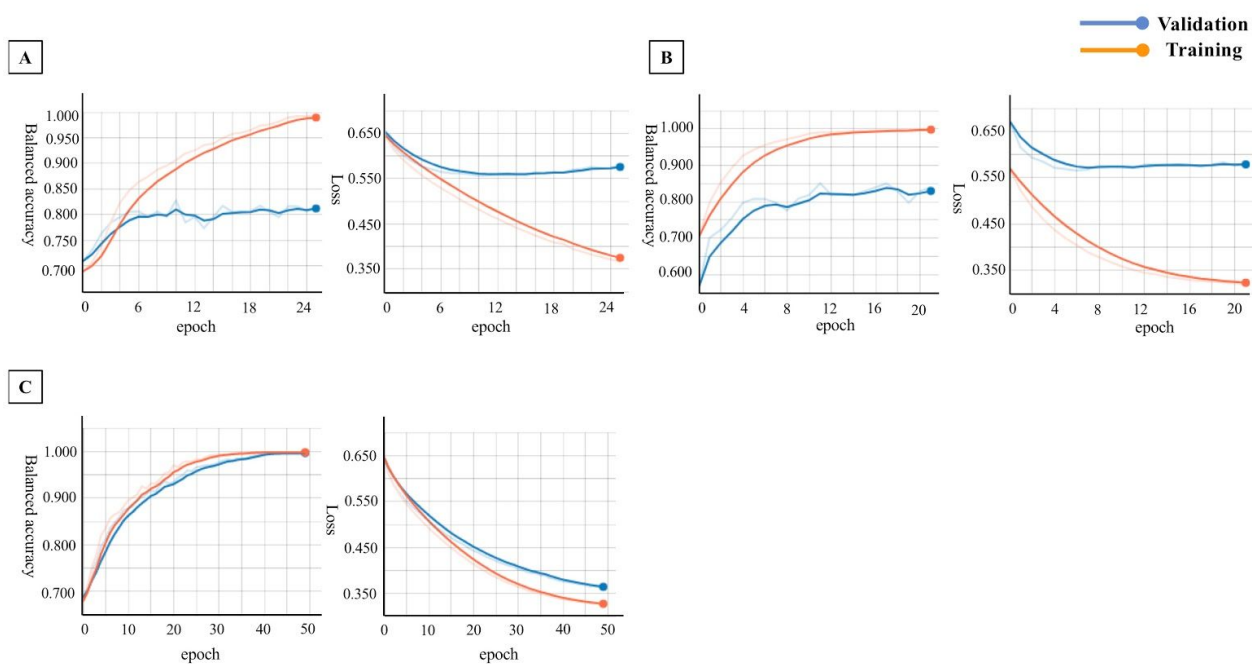


eFigure 4. Training process monitoring for 2D slice-level CNN

Training and validation accuracy/loss during the training process were evaluated after each epoch. The accuracy and loss curves were smoothed with a threshold (0.6).

For each plot a subfigure letter is used and the corresponding information on the experiment may be found in the table below or in eTable 4 according to the “Experiment number”.

Subfigure	Experiment number	Fold displayed	Epoch where training stopped	Epoch of the highest validation accuracy	Highest validation accuracy
A	18	2	21	11	0.85
B	19	2	15	15	0.84
C	20	2	49	49	1.00



References

- Ellis, K.A. et al., 2010. Addressing population aging and Alzheimer's disease through the Australian Imaging Biomarkers and Lifestyle study: Collaboration with the Alzheimer's Disease Neuroimaging Initiative. *Alzheimer's & Dementia*, 6(3), pp.291–296. Available at: <http://dx.doi.org/10.1016/j.jalz.2010.03.009>.
- Ellis, K.A. et al., 2009. The Australian Imaging, Biomarkers and Lifestyle (AIBL) study of aging: methodology and baseline characteristics of 1112 individuals recruited for a longitudinal study of Alzheimer's disease. *International Psychogeriatrics*, 21(04), p.672. Available at: <http://dx.doi.org/10.1017/s1041610209009405>.
- Marcus, D.S. et al., 2007. Open Access Series of Imaging Studies (OASIS): cross-sectional MRI data in young, middle aged, nondemented, and demented older adults. *Journal of cognitive neuroscience*, 19(9), pp.1498–1507.
- McKhann, G. et al., 1984. Clinical diagnosis of Alzheimer's disease Report of the NINCDS-ADRDA Work Group* under the auspices of Department of Health and Human Services Task Force on Alzheimer's Disease. *Neurology*, 34(7), pp.939–939.
- Petersen, R.C. et al., 2010. Alzheimer's Disease Neuroimaging Initiative (ADNI): clinical characterization. *Neurology*, 74(3), pp.201–209.
- Winblad, B. et al., 2004. Mild cognitive impairment—beyond controversies, towards a consensus: report of the International Working Group on Mild Cognitive Impairment. *Journal of internal medicine*. Available at: <https://onlinelibrary.wiley.com/doi/abs/10.1111/j.1365-2796.2004.01380.x>.